NAVAL POSTGRADUATE SCHOOL
MONTEREY, CA 93940

# NAVAL POSTGRADUATE SCHOOL
## Monterey, California

# THESIS

TROPICAL DISTURBANCES IN AN OCEANIC
GENERAL CIRCULATION MODEL
WITH SEASONAL FORCING

by

Richard Duane LeRoy

June 1979

Thesis Advisor: R. L. Haney

Approved for public release; distribution unlimited.

T189130

SECURITY CLASSIFICATION OF THIS PAGE (When Data Entered)

# REPORT DOCUMENTATION PAGE

READ INSTRUCTIONS BEFORE COMPLETING FORM

1. REPORT NUMBER

2. GOVT ACCESSION NO.

3. RECIPIENT'S CATALOG NUMBER

4. TITLE (and Subtitle)
Tropical Disturbances in an Oceanic General Circulation Model with Seasonal Forcing

5. TYPE OF REPORT & PERIOD COVERED
Master's Thesis; June 1979

6. PERFORMING ORG. REPORT NUMBER

7. AUTHOR(s)
Richard Duane LeRoy

8. CONTRACT OR GRANT NUMBER(s)

9. PERFORMING ORGANIZATION NAME AND ADDRESS
Naval Postgraduate School
Monterey, California 93940

10. PROGRAM ELEMENT, PROJECT, TASK AREA & WORK UNIT NUMBERS

11. CONTROLLING OFFICE NAME AND ADDRESS
Naval Postgraduate School
Monterey, California 93940

12. REPORT DATE
June 1979

13. NUMBER OF PAGES
67

14. MONITORING AGENCY NAME & ADDRESS(if different from Controlling Office)

15. SECURITY CLASS. (of this report)
Unclassified

15a. DECLASSIFICATION/DOWNGRADING SCHEDULE

16. DISTRIBUTION STATEMENT (of this Report)
Approved for public release; distribution unlimited.

17. DISTRIBUTION STATEMENT (of the abstract entered in Block 20, if different from Report)

18. SUPPLEMENTARY NOTES

19. KEY WORDS (Continue on reverse side if necessary and identify by block number)

20. ABSTRACT (Continue on reverse side if necessary and identify by block number)

A ten-level primitive equation ocean circulation model is used to investigate the formation and propagation of baroclinic wavelike responses to annual variations in wind stress forcing. At 12.2°N a thermal response to Ekman pumping is observed to be in phase across the entire longitudinal extent of the model Pacific Ocean. A zonal fluctuation in interior ocean current systems is also suggested. Eastern boundary

DD FORM 1 JAN 73 1473 EDITION OF 1 NOV 65 IS OBSOLETE
(Page 1) S/N 0102-014-6601

disturbances not related to local forcing are observed to propagate poleward. At 6.1°N, main thermocline displacements are observed to propagate westward as the result of vertical advection induced by Ekman pumping. Surface layer temperature disturbances also exist which are produced by meridional advection of mean temperature (colder to the south) by surface Ekman currents. Eastern boundary disturbances also exist at this latitude and extend to a deeper level. All disturbances observed in this investigation are considered to be permanent features of the model circulation. Grid size limitations preclude detailed investigation of the observed boundary disturbances with this model.

Approved for public release; distribution unlimited.

# Tropical Disturbances in an Oceanic General Circulation Model with Seasonal Forcing

by

Richard Duane LeRoy
Lieutenant, United States Navy
B.S., Purdue University, 1971

Submitted in partial fulfillment of the requirements for the degree of

MASTER OF SCIENCE IN METEOROLOGY AND OCEANOGRAPHY

from the

NAVAL POSTGRADUATE SCHOOL
June 1979

NAVAL POSTGRADUATE SCHOOL
MONTEREY, CA 93940

## ABSTRACT

A ten-level primitive equation ocean circulation model is used to investigate the formation and propagation of baroclinic wavelike responses to annual variations in wind stress forcing. At 12.2°N a thermal response to Ekman pumping is observed to be in phase across the entire longitudinal extent of the model Pacific Ocean. A zonal fluctuation in interior ocean current systems is also suggested. Eastern boundary disturbances not related to local forcing are observed to propagate poleward. At 6.1°N, main thermocline displacements are observed to propagate westward as the result of vertical advection induced by Ekman pumping. Surface layer temperature disturbances also exist which are produced by meridional advection of mean temperature (colder to the south) by surface Ekman currents. Eastern boundary disturbances also exist at this latitude and extend to a deeper level. All disturbances observed in this investigation are considered to be permanent features of the model circulation. Grid size limitations preclude detailed investigation of the observed boundary disturbances with this model.

TABLE OF CONTENTS

I. INTRODUCTION - - - - - - - - - - - - - - - - - - - - 10

II. DATA SOURCES AND PROCESSING - - - - - - - - - - - 13

III. OBSERVATIONS AND RESULTS - - - - - - - - - - - - 16

IV. CONCLUSIONS - - - - - - - - - - - - - - - - - - - 31

LIST OF REFERENCES - - - - - - - - - - - - - - - - - - 65

INITIAL DISTRIBUTION LIST - - - - - - - - - - - - - - 67

LIST OF FIGURES

1. Meridional Gaussian smoothing function used over the surface wind stress field as described in text - - - - - - - - - - - - - - - - - - - 33

2. Annual mean surface wind stress vectors over the model domain. Stress vectors are plotted at alternate grid points with the length of the arrow directly proportional to the magnitude of the stress - - - - - - - - - - - - - - - - - 34

3. Curl of the surface wind stress for a typical spring month (April) as used in the model. Contour interval is 5 x $10^{-3}$ $N/m^3$. Hatched areas represent positive values - - - - - - - - - 35

4. Same as Figure 3 except for a typical fall month (October) - - - - - - - - - - - - - - - - - - 36

5. Time-longitude map of the departure from the annual mean of the zonal (u') flow across 12.2°N at 162.5 m (level 5). Contour interval is 0.4 cm/s. Hatched areas represent positive values - - - - - - - - - - - - - - - - - - 37

6. Same as Figure 5 except for meridional (v') flow - - - - - - - - - - - - - - - - - - - - - - 38

7. Same as Figure 5 except for vertical velocity (w'). Contour interval is 2.0 cm/day - - - - - - - 39

8. Time-latitude map of the departure from the annual mean of vertical velocity (w') along the model eastern boundary (125°W) at level 5. Contour interval is 30.0 cm/day. Hatched areas represent positive values - - - - - - - - - - 40

9. Same as Figure 5 except for temperature (T'). Contour interval is 0.1°C - - - - - - - - - - - - - 41

10. Same as Figure 5 except for Ekman pumping velocity. Contour interval is 4.0 cm/day - - - - 42

11. Vertical cross section (x,z) of the departure from the annual mean of the zonal flow (u') across 12.2°N on August 3 of the last model year. Contour interval is 0.4 cm/s. Hatched areas represent positive values - - - - - - - - - 43

12. Same as Figure 11 except for meridional (v') flow - - - - - - - - - - - - - - - - - - - - - - - 44

13. Same as Figure 11 except for vertical velocity (w'). Contour interval is 5.0 cm/day - - - - - - - 45

14. Same as Figure 11 except for temperature (T'). Contour interval is 0.1°C - - - - - - - - - - - - - 46

15. Time depth map of the departure from the annual mean of the zonal (u') flow at latitude 12.2°N and longitude 162°W. Contour interval is 0.5 cm/s. Hatched areas represent positive values - - - - - - - - - - - - - 47

16. Same as Figure 15 except for meridional (v') flow - - - - - - - - - - - - - - - - - - - - - - - - 48

17. Same as Figure 15 except for vertical velocity (w'). Contour interval is 2.0 cm/day - - - - - - - 49

18. Same as Figure 15 except for temperature (T'). Contour interval is 0.1°C - - - - - - - - - - - - - 50

19. Time-longitude map of the departure from the annual mean of the zonal (u') flow across 6.1°N at level 5. Contour interval is 0.4 cm/s. Hatched areas represent positive values - 51

20. Same as Figure 19 except for meridional (v') flow - - - - - - - - - - - - - - - - - - - - - - - - 52

21. Same as Figure 19 except for vertical velocity (w'). Contour interval is 2.0 cm/day - - - - - - - 53

22. Same as Figure 19 except for temperature (T'). Contour interval is 0.1°C - - - - - - - - - - - - - 54

23. Same as Figure 19 except for Ekman pumping velocity. Contour interval is 4.0 cm/day - - - - 55

24. Vertical cross section (x,z) of the departure from the annual mean of the zonal (u') flow across 6.1°N on August 3 of the last model year. Contour interval os 0.4 cm/s. Hatched areas represent positive values - - - - - - - - - 56

25. Same as Figure 24 except for meridional (v') flow - - - - - - - - - - - - - - - - - - - - - - - - 57

26. Same as Figure 24 except for vertical velocity (w'). Contour interval is 5.0 cm/day - - - - - - - 58

27. Same as Figure 24 except for temperature (T'). Contour interval is 0.1°C - - - - - - - - - - - - - 59

28. Time depth map of the departure from the annual mean of the zonal (u') flow at latitude 6.1°N and longitude 162°W. Contour interval is 0.5 cm/s. Hatched areas represent positive values - - - - - - - - - - - - 60

29. Same as Figure 28 except for meridional (v') flow - - - - - - - - - - - - - - - - - - - - - - - - 61

30. Plots of the zonal ($\tau_x'$) and meridional ($\tau_y'$) components of wind stress as functions of time at latitude 6.1°N and longitude 162°W - - - 62

31. Same as Figure 28 except for vertical velocity (w'). Contour interval is 2.0 cm/day - - - - - - 63

32. Same as Figure 28 except for temperature (T'). Contour interval is 0.1°C - - - - - - - - - - - - 64

ACKNOWLEDGEMENTS

The author wishes to express his appreciation to Dr. Robert L. Haney for his guidance, patient understanding and counsel in the preparation of this thesis and to Dr. C. P. Chang for reading the thesis and making valuable comments.

# I. INTRODUCTION

Recent modeling investigations of the strength and thermal structure of Tropical North Pacific Ocean currents have provided evidence as to the existence of a baroclinic response to annual variations in wind stress. Meyers (1978) has observed variations in the depth of the 14°C isotherm which, at 6°N, propagate westward at nearly the speed of free, non-dispersive Rossby waves. His model mechanisms at 6°N are Ekman layer divergence (Ekman pumping) as a response to local wind stress, and planetary, geostrophic divergence inherent on a rotating sphere. At 10°N Meyers observed thermocline depth variations which were nearly in phase across the Pacific with the Ekman pumping velocity calculated from the local wind stress. White (1977) found an agreement in phase only at 130°W, and suggested a baroclinic response to annual forcing in the form of a long wave which results from the superposition of baroclinic Rossby waves emanating from the eastern boundary, and the local forced response. This resulting long wave propagated at twice the speed of free Rossby waves.

The purpose of this study was to investigate further any low frequency responses to wind forcing in the North Equatorial Pacific and to consider whether any such responses are consistent with theory. The numerical model used is that of Haney (1974) with subsequent improvements involving

parameterization of convective mixing and surface wind stirring (Haney and Davies, 1976) and nonlinear eddy viscosity (Haney and Wright, 1975). This model is based on the hydrostatic and Boussinesq approximations and is a 10-level primitive equation model in a closed rectangular basin with a uniform depth of 4 kilometers. The model basin extends from the equator to 65°N and westward for 90° of longitude from 125°W. Horizontal resolution is approximately 3° of longitude and 2° of latitude with 33 uniformly spaced grid points in both the east-west and north-south directions. The ten vertical levels are placed at 10, 32.5, 62.5, 102.5, 162.5, 462.5, 900, 1700, and 3100 meters below the undisturbed sea surface. The model has been developed and improved in order to study large-scale thermal anomalies observed in the Central North Pacific Ocean by the North Pacific Experiment (NORPAX).

The model was "spun up" for a number of years of simulated time sufficient to allow circulations and thermal patterns to establish themselves and then detailed analysis of the transient response in the tropical regions was made. The wind stress prescribed as a forcing function in the model from the equator to 30°N was that used by Meyers (1978) and described in detail by Wyrtki and Meyers (1975). North of 30°N wind stress was calculated from geostrophic wind data obtained from an NCAR data tape of the Northern Hemisphere climatological atlases of Jenne et al., (1969a, b). The major region of interest was south of 20°N. This location

was where Meyers and White observed wavelike disturbances and it was reasonable to expect similar waves in this study. By analyzing any observed waves as to their phase relationship with the local wind stress curl, their phase speed, and their wavelength, possible mechanisms for their generation and propagation may be suggested and compared with theory.

By better understanding how the oceanic circulation changes as a result of variant wind forcing, more comprehensive studies of large-scale air-sea interaction and climatic changes may be undertaken.

## II. DATA SOURCES AND PROCESSING

Data from two different sources, one covering the region north of 30°N, and one covering the region south of 30°N, were combined to produce a realistic wind stress field which was used as a forcing function in this modeling investigation. The first data base was that processed and explained in detail by Wyrtki and Meyers (1975). This monthly averaged wind stress data, sorted into 2° latitude by 10° longitude fields encompassing 29°S to 29°N and 125°E to 75°W, was generously provided by Dr. Steve Piascek of NORDA. Only the data which was appropriate for use by the model, i.e. that data from the equator northward and from 145°E to 125°W, were used in this study. Wyrtki and Meyers calculated these stress data for each observation according to the formula

$$\{\tau^{\lambda}, \tau^{\phi}\} = \rho_a \, c_d \, |\vec{V}_a| \, (u_a, v_a)$$

where $\tau$ is the wind stress, rectangular component positive to the east ($\lambda$) and north ($\phi$), $\rho_a$ is the constant surface air density of 1.2 kg/m$^3$, $c_d$ is the drag coefficient assumed constant in the trade wind zone at $1.5 \times 10^{-3}$, $u_a$ and $v_a$ are the surface wind components, and $|\vec{V}_a| = (u_a^2 + v_a^2)^{\frac{1}{2}}$, the magnitude of the surface wind. A quadratic interpolation scheme was used to transfer the Wyrtki-Meyers monthly wind stress component arrays, extending from the equator to 29°N, to the model gridpoints.

The second source of data was an NCAR tape of monthly mean climatological surface geostrophic wind component data (Jenne et al., 1969a, b). These wind components had been sorted into $5^{\circ}$ latitude by $5^{\circ}$ longitude fields encompassing the model latitudes and ranging in longitude from $120^{\circ}$E to $80^{\circ}$W. These data were used to calculate surface wind stress using the same formula as above. However, an atmospheric drag coefficient of $1.3 \times 10^{-3}$ was used (Businger et al., 1971) and a 10% reduction in magnitude from geostrophic was assumed. The resulting stress components for the model domain north of $30^{\circ}$N were interpolated to model gridpoints.

By combining the stress component fields computed and/or interpolated from the two data sources, 33 x 33 fields encompassing the model's geographical domain for individual months were obtained. The Wyrtki-Meyers stress data, included from the equator to $29^{\circ}$N, is based on actual wind observations in the tropics, while the NCAR data, from $30^{\circ}$N to the northern boundary, is based on geostrophic wind calculations from monthly mean sea-level pressure data. It is felt that the resulting stress field represents the best total stress pattern that is presently available from monthly mean data over the North Pacific Ocean.

Although the major feature of the two stress fields matched quite well at the common latitude of $30^{\circ}$N, a smoothing technique was employed to remove small scale irregularities and improve horizontal consistency. A weighted three-point meridional average given by

$$\tau^{*}_{i,j} = \tau_{i,j} + .25(\tau_{i,j+1} - 2\tau_{i,j} + \tau_{i,j-1})\, W_j$$

was selected with the weight, $W_j$, a Gaussian function of the latitude (i is the longitudinal gridpoint index and j is the latitudinal index). $W_j$ is detailed and illustrated in Figure 1. At the interface between the two data sources, $30^{\circ}$N, $W_j$ approaches one, and at the latitudinal boundaries of the model it approaches zero. Essentially, then, at the interface the smoothing process was a $\frac{1}{4}$, $\frac{1}{2}$, $\frac{1}{4}$ meridional filter, and near the boundaries was negligible. The meridional smoothing was performed twice with boundary values being unchanged. Additionally, a $\frac{1}{4}$, $\frac{1}{2}$, $\frac{1}{4}$ monthly time filter was used once over the entire fields and is given by

$$\tau^{s}_{i,j,k} = .25(\tau_{i,j,k-1} + 2\tau_{i,j,k} + \tau_{i,j,k+1}),$$

where k indicates the month.

The ocean circulation model (Haney et al., 1978) was integrated over a total of nine complete annual cycles starting from the results of the previous model. The only change from the previous model is the introduction of the new wind stress fields as described above. After nine years of integration it was clear that the upper layers of the ocean model, i.e. those most strongly affected by the annual variation in wind forcing, were essentially repeating themselves one year after another. The results analyzed below are those from the eighth and ninth years of the nine year integration. Primary attention is devoted to the annual variation of model variables, less to the annual mean.

## III. OBSERVATIONS AND RESULTS

The trade wind field over the Pacific Ocean is one of the largest and most consistent wind fields on earth although little is actually known about its time and spacial fluctuations (Wyrtki and Meyers, 1976). Wind-driven ocean circulation studies are largely dependent on wind stress field fluctuations since the curl of the wind stress, and thus Ekman surface layer divergence or pumping, is a very crucial forcing parameter. Accordingly, maps of the surface wind stress and of its curl were analyzed for significant fluctuations which may be related to observable oceanic disturbances.

Figure 2 is a depiction of the annual mean wind stress vectors over the model domain. The region of primary interest in this investigation is that south of $20^{\circ}$N. As shown, the Intertropical Convergence Zone (ITCZ) has an annual mean position at about $8^{\circ}$N. Wyrtki and Meyers (1975) have shown that the curl of the wind stress and thus the Ekman pumping velocity is relatively insensitive to changes in wind strength and depend mostly on the locations of strong meridional shear, which show latitudinal variation throughout the year. In the northern hemisphere winter and spring, the northeast trades are at their strongest and the southeast trades at their weakest. The ITCZ lies about $3^{\circ}$ south of its annual mean position and as seen in Figure 3, a map of

wind stress curl for a typical spring month, regions of strong positive wind stress curl appear between $5^{o}N$ and $10^{o}N$. Two zones of particularly strong positive curl are apparent, one between $155^{o}E$ and $175^{o}E$ and another between $155^{o}W$ and $140^{o}W$. In the northern hemisphere summer and fall, the ITCZ shifts northward to about $13^{o}N$ and the zone of strongest cyclonic curl is located between $10^{o}N$ and $15^{o}N$ as seen in Figure 4.

The strongest meridional shear in the surface wind stress is observed in a band slightly north of the ITCZ which passes over the annual mean position of the ITCZ twice per year. Therefore the amplitude of the first annual variation of the shear is largest at the latitudinal extremes of the ITCZ and small at the annual mean position. Meyers (1978) computed the amplitude of the first annual harmonic of the Ekman pumping velocity and the depth of the $14^{o}C$ isotherm in the North Pacific and found that both reached maxima at $6^{o}N$ and at $10^{o}N$. Not surprisingly, these latitudes coincided with the zones of strongest cyclonic wind stress curl. As mentioned previously, at $10^{o}N$ the Ekman pumping velocity and the depth of the $14^{o}C$ isotherm fluctuated in phase across the Pacific while at $6^{o}N$ the temperature fluctuations propagated westward from a region of resonant forcing in the Eastern Pacific. In order to analyze results which could best be compared with those of Meyers (1978), model latitudes of $6.1^{o}N$ and $12.2^{o}N$ were chosen for study in this investigation.

a. Results at 12.2°N

Meyers' (1978) result at 10°N was an oceanic temperature response which was nearly in phase (a two month zonal lag) with the local Ekman pumping velocity across the entire Pacific Ocean. White (1977) theorized that the annual fluctuation at any interior ocean location from 10°N to 20°N depends on the fluctuating wind field over the entire eastward ocean with the phase speed and amplitude strongly related to distance from the eastern boundary. In a bounded ocean, the presence of the eastern boundary can significantly alter the phase distribution of the oceanic response to Ekman pumping by acting as a concentrated source of baroclinic planetary waves which propagate boundary responses westward into the interior, drastically altering the phase relation predicted by local forcing only (White, 1977).

Model level 5, corresponding to a depth of 162.5 meters, was chosen for detailed study since it is the model level which most closely corresponds with the observed depth of the 14°C isotherm (Meyers, 1978). This level is above the intermediate layers where the vertical temperature gradient is weak and below the level of the maximum density gradient, whose stability shields it from temperature fluctuations associated with sea surface heat exchanges. Time-longitude maps of departures from the annual mean (denoted with a prime) of the zonal (u') and meridional (v') flow, vertical velocity (w'), and temperature (T') were developed to show any zonal propagation of wavelike disturbances. Figures 5 and 6 are such maps of u' and v' respectively at level 5 across 12.2°N

over the last two years of the model run. These figures indicate westward propagating annual signals which emanate from near or at the eastern boundary with the zonal component having a slightly faster phase speed and a higher magnitude. Figure 7 is a similar depiction of the disturbance vertical velocity, w'. The major features of the open ocean vertical velocity field in Figure 7 develop near the eastern boundary and seem to propagate westward as far as the mid ocean region at which point further westward propagation with increasing time is not observed. White (1977) observed that due to the inverse latitudinal dependence in zonal phase speed, baroclinic long waves in the eastern ocean are directed westward while in the western ocean they appear to be directed more northward due to refraction effects. Regardless, the overall pattern observed in Figure 7 does not correlate with those of the zonal and meridional flow components shown in Figures 5 and 6 respectively. Vertical velocity is generally related to the divergent part of the flow; the propagating features of Figures 5 and 6 are most likely due to the rotational part of flow and as such have little impact on the vertical velocity. It is noted that disturbances in Figures 5 through 7 appear to intensify along the western boundary of the model ocean. This is to be expected since westward propagating features tend to congregate at or near western boundaries in models such as that used in this study.

Figure 7 also shows local disturbances of great intensity along the eastern boundary. However, these disturbances do not appear to propagate westward to any significant extent.

They also do not appear to be related to the longshore (meridional) component of wind stress nor to local Ekman pumping. In order to investigate any meridional propagation of these boundary features, a time-latitude map of w' along the eastern boundary was prepared and is shown in Figure 8. Wyrtki (1975) has surmised that the annual baroclinic response at an eastern boundary away from the equator is in part composed of a perturbation which propagates into the region from the equatorial region in the form of an internal Kelvin wave. Those coastal disturbances at 12.2°N in Figure 8 have a computed (northward) phase speed of 11.7 cm/s and the major features have an annual period. It is interesting to note that Enfield and Allen (1978) have recently observed spatially coherent disturbances in monthly mean anomalies of temperature and sea level along the Pacific coast of North and South America. In the tropical latitudes, these observed fluctuations are also uncorrelated with local forcing mechanisms and propagate poleward at phase speeds comparable to those obtained in the model (Allen, personal communication). Because of the coarse grid in the present model however, no further comparison between model results and coastal observations is justified.

Another important result which can be seen from Figures 5 through 8, and others below, is that the two consecutive model years are virtually identical. This means that the model is in a statistical equilibrium with the forcing and that the oscillations being examined are not transitory but are permanent features of the model circulation.

Figure 9 is a time-longitude map of temperature disturbances which is very consistent with the vertical velocity pattern given in Figure 7. A two month phase lag is apparent with generally warm water sinking during the first half of the year and cold water rising during the second half - clearly and indirect, thermally forced disturbance. Calculations based on the annual positive disturbance in the east-central ocean in Figure 9 revealed a zonal wavelength of about 10,000 kilometers and a zonal phase speed of approximately -42 cm/s. These results are in qualitative agreement with White (1977) who theorized a wavelength of 10,000 kilometers and a phase speed of -32 cm/s and observed a wavelength of 16,000 kilometers and a phase speed of -46 cm/s at $12^{\circ}$N.

The Ekman pumping velocity was calculated from the following formula as described in detail by DeWitt and Leetmaa (1978)

$$W_{-h} = \int_{-h}^{0} (u_x + v_y)\, dz.$$

A map of the disturbance Ekman pumping velocity is presented in Figure 10. This pattern corresponds with the gross features of the vertical velocity field of Figure 7 although no propagation is noted in the eastern ocean. This is in contrast with the results of both White (1977) and DeWitt and Leetmaa (1978) who noticed a tendency for the Ekman pumping disturbances to propagate westward. Magnitude differences between corresponding features in Figures 7 and 10 are perhaps

due to the fact that Figure 10 represents the depth of the bottom of the Ekman layer which need not be coincident with level 5 of the model. Additionally, different processes are involved in vertical velocity and Ekman pumping. The theoretical Ekman depth was calculated according to the formula

$$D_e = \pi\left(\frac{2K_m}{f}\right)^{\frac{1}{2}}$$

(DeWitt and Leetmaa, 1978) where $K_m$ is the vertical eddy viscosity coefficient in the model which is 10 $cm^2/s$, and f is the Coriolis parameter. At 12.2°N, this depth was calculated to be approximately 20 meters.

In order to describe the vertical structure of the annual wave disturbances, vertical cross sections (x,z) of the disturbance quantities were prepared across 12.2°N on August 3 of the last model year. This date was selected so as to coincide with the large positive amplitude disturbance noted on the time-longitude section of Ekman pumping in Figure 10. Figure 11, the vertical cross section of u' on August 3, may be compared with the time-longitude map of u' in Figure 5. The positive wavelike disturbance near the eastern boundary in Figure 5 extends from the surface to the bottom with greatest magnitude near the surface, as is the case with the positive disturbance in the western ocean. The negative disturbance in the mid-ocean extends from the surface to about 1500 meters with greatest magnitude at about 50 meters. The result that the largest magnitudes are not at the surface in Figure 11 may be explained by the dependence of the zonal

flow on temperature and pressure gradient structure and not so much on the surface winds. Generally, then, the zonal disturbances extend quite deep at their formative stage and do not significantly deepen or shoal as they propagate westward.

Figure 12 shows the corresponding cross section of the meridional velocity perturbation which may be compared with the time-longitude section of Figure 6. The positive disturbance in the mid-western ocean in Figure 6 on August 3 extends vertically to within about 50 meters of the surface. The negative disturbance in the eastern ocean extends from about 1500 meters to the surface where it expands to cover the entire model domain across 12.2°N. The negative disturbance is of greatest magnitude near the surface at all longitudes while the positive disturbance is very small whenever it appears. Apparently the meridional flow component is more closely related to the surface winds than is the zonal component.

Figure 13 depicts the vertical-zonal cross section of vertical velocity disturbance across 12.2°N on August 3. The positive disturbance in Figure 7 encompasses most of the model domain except for the surface layer and the extreme eastern boundary. Largest magnitudes are centered at depths of about 1000 meters. The eastern boundary negative disturbance extends from about 200 meters to the surface.

Corresponding temperature disturbances are shown in Figure 14. Warm conditions are noted in all areas on August 3 except the eastern region at levels below about 75 meters.

Wunsch (1977) has noted that if wind forcing is assumed to be over an annual period then there is no reason to isolate the problem of vertical propagation from that of horizontal. He contends that internal gravity waves will determine the vertical modal structure and that in the presence of a non-dissipative and flat bottom energy may travel from the surface to the bottom and then be reflected back to the surface. Any vertical propagation of wavelike disturbances should be apparent in time-depth maps of the perturbation quantities. These depictions were developed and are shown in Figures 15 through 18. These maps were made at an arbitrarily selected interior ocean longitude of 162°W. No vertical propagation is seen in the zonal and meridional velocity components, Figures 15 and 16 respectively. Again it can be seen that u' penetrates deeper than v' and is therefore most likely due to the north-south meandering of the major equatorial current systems which are primarily zonal. Figure 17 reveals that the vertical velocity disturbances also do not appear to propagate vertically but they attain their greatest magnitudes at fairly substantial depths. These deep centers apparently are the cause of the corresponding deep temperature disturbances (Figure 18) which lag the vertical velocity by about 2½ months. The temperature fluctuations above 150 meters are due to the seasonal cycle of surface heat flux modified slightly by a fluctuating meridional temperature advection in the upper 50 meters. Again notice how the two model years are nearly identical - thus in equilibrium with the forcing.

The model results at 12.2°N are summarized as follows. The dominant thermal response at the depth of the main thermocline occurs in phase across the entire longitudinal extent of the ocean and is attributed to large scale vertical advection produced by wind-induced Ekman pumping. This is in agreement with the theoretical analysis and observational results of Meyers (1978). In addition, there is a pronounced fluctuation in the zonal current in the open ocean which appears to be associated with a north-south seasonal meandering of the main zonal current systems. There also exists poleward propagating disturbances confined to the immediate vicinity of the eastern boundary which do not appear to be related to the local forcing. Further study is required to determine whether these disturbances are in any way related to the sea level disturbances observed along the North American coast by Enfield and Allen (1978).

b. Results at 6.1°N

Variations in the depth of the 14°C isotherm which propagated westward at nearly the phase speed of free non-dispersive Rossby waves were observed at 6°N by Meyers (1978). He theorized that the waves were generated by the zonal and seasonal variability in Ekman layer divergence in the eastern Pacific and that they propagated nearly freely in the western Pacific where he found the forcing was weak. The resulting wave lagged the Ekman pumping velocity by slightly more than one month at the position of maximum forcing.

Figures 19 and 20 are time-longitude maps of zonal and meridional flow disturbances, u' and v' respectively, across 6.1°N at 162.5 m (model level 5) during the same two model years analyzed above at 12.2°N. These figures indicate rapidly westward propagating annual signals which appear to emanate from the eastern boundary. The zonal component in Figure 19 appears to increase gradually in magnitude to a maximum in the region slightly west of the mid-ocean and then decreases from there to the western boundary. The zonal disturbances propagate faster than the meridional and faster at 6.1°N than at 12.2°N (Figure 5). Figure 21 is a time-longitude map of vertical velocity disturbance at the same latitude and depth. As was noted for Figure 7 at 12.2°N, local disturbances of great magnitude are observed along the eastern boundary which do not appear to propagate westward. These northerly propagating Kelvin-like disturbances (it can be seen from Figures 19 through 22 that v', T', and w' are involved in the disturbance but not u') are depicted in Figure 8. Near the eastern boundary in Figure 21, wavelike perturbations form and propagate completely across the model domain, in contrast with those at 12.2°N (Figure 7) which appear to be nearly in phase across the ocean. The disturbances' amplitudes slowly vary with westward propagation.

The temperature disturbance at 6.1°N (Figure 22) has essentially the same pattern as the vertical velocity disturbance but with a two month phase lag which indicates the temperature is responding to the vertical velocity. Calculations revealed a phase speed of -32 cm/s, a zonal

wavelength of about 9900 kilometers, and an annual period. Meyers (1978) observed a corresponding phase speed of -56 cm/s with a wavelength of 17,000 kilometers at $6^{o}$N.

A time-longitude map of Ekman pumping velocity disturbance across $6.1^{o}$N is shown in Figure 23. The theoretical Ekman depth as calculated above for $12.2^{o}$N was found to be approximately 28 meters at $6.1^{o}$N. The pattern in Figure 23 correlates well with the actual vertical velocity (Figure 21) which in turn correlates with the temperature fields except for the region of very slow westward propagation in the mid-ocean area. Propagation is very rapid in both the eastern and western thirds with greatest amplitudes observed at the eastern boundary ($125^{o}$W). The latter observation is consistent with Meyers' (1978) finding that the maximum displacement occurs at $130^{o}$W. The region of strong cyclonic wind stress curl observed at this latitude in Figure 3 was at and slightly west of $140^{o}$W.

The zonal-depth structure of the disturbance patterns across $6.1^{o}$N on August 3 of the last model year is depicted in Figures 24 through 27. Figure 24 shows that the positive u' disturbance of Figure 19 is very broad at great depths, narrow at mid levels, and widens again in the surface layers with slightly higher magnitudes observed at the surface. The corresponding negative disturbance is widest and has its greatest magnitude at about 75 meters. As was discussed previously with regard to Figure 11, there is a deep zonal current fluctuation which seems to be related to the north-south displacement of the main current systems which are

zonal. The meridional velocity disturbance across 6.1°N is presented in Figure 25. A relatively weak flow is predominant across the model domain except in the surface layers where, as in Figure 12, there is a strong response due to the dependence on surface winds. Positive disturbances shown in Figure 25 are of much smaller magnitude.

The zonal-depth map of w' in Figure 26 shows that with the exception of a narrow semi-vertical band in the western ocean and the Kelvin-like disturbances on the eastern boundary, the model domain is predominantly occupied by sinking ($w' < 0$) disturbances at this time. The shallow Kelvin disturbance extends deeper at 6.1°N than it did at 12.2°N (Figure 13) and a phase change is apparent between the two latitudes. Figure 27 shows that the model domain is colder than normal except for the eastern ocean surface layer and a mid-level warm disturbance in the western ocean.

Time-depth maps of u' and v' at 162°W are shown in Figures 28 and 29. Disturbances of greatest magnitudes occur at the surface with those of the zonal component extending quite deep. On comparing these figures with their counterparts at 12.2°N, Figures 15 and 16, the differences in disturbance magnitudes between the two latitudes is obvious; the deep response is a little stronger at 6.1°N but the surface Ekman flow is nearly an order of magnitude higher at 6.1°N. Plots of the disturbances of the zonal and meridional components of wind stress as functions of time at 162°W are shown in Figure 30. The large magnitude surface layer disturbances noted in Figures 28 and 29 are in phase with these

stress disturbances indicating that the wind stress is most likely the dominant forcing process of ocean (Ekman) flow at the surface and immediately below. The time-depth map of vertical velocity disturbance across 6.1°N as presented in Figure 31 is similar to that of 12.2°N (Figure 17) in that greatest magnitudes are reached at deep levels. However, in contrast to 12.2°N, there is a phase shift at intermediate levels at 6.1°N. The phase shift probably represents a transition region between the upper 500 meters or so, which is responding to the wind, and the remainder of the ocean which is reacting out of phase. Figure 32 shows the strong response of the temperature field in the upper 500 meters to the vertical motion with a two month lag. At the same time, surface disturbances due to seasonal wind changes occur but they are confined to the upper 50 meters. At 6.1°N v' advects cold water northward from the equatorial surface region during the first half of the year and warm water southward during the second half of the year.

The model results at 6.1°N are summarized as follows. The dominant thermal response in the vicinity of the main thermocline (level 5, or 162.5 meters in the model) is a westward propagating disturbance (Figure 22) produced by vertical advection (w' in Figure 21) induced by Ekman pumping (Figure 23). Figure 27 shows that the temperature response seen at 162.5 meters involves the entire thermocline and is actually strongest at about 100 meters. In addition to the propagating thermal response in the main thermocline there is an equally pronounced annual cycle of surface temperature (Figure 32)

which is produced primarily by meridional advection of mean temperature (colder to the south) by surface Ekman currents (Figure 29).

# IV. CONCLUSIONS

Wavelike features simulated in the tropical regions of an ocean circulation model which are seen as disturbances from the annual mean of vertical velocity and temperature have been described. These features are considered to be permanent oscillations of the model circulation and result from variability in wind stress forcing. At 12.2°N, a thermal response to large scale vertical advection produced by wind-induced Ekman pumping or surface layer divergence occurs practically in phase across the entire longitudinal extent of the model ocean. Underlying features of the annual signal do appear to propagate westward. These results are in agreement with the theory and observations of Meyers (1978). Evidence also suggests a zonal fluctuation in the interior ocean current systems. Along the eastern boundary poleward propagating perturbations of the vertical velocity field exist which may be related to sea level disturbances which have been observed by Enfield and Allen (1978).

At 6.1°N, thermocline displacements propagate westward also as a result of vertical advection induced by Ekman pumping. Disturbances at this latitude are significantly higher in magnitude than those observed at 12.2°N. Additionally, pronounced sea surface temperature disturbances are apparently produced by meridional advection of mean temperature by

surface Ekman currents. Eastern boundary perturbations also exist and extend deeper at 6.1°N than at the higher latitude.

Results and observations in this study were generally consistent with accepted theory. It would be beneficial to consider latitudes other than 6.1°N and 12.2°N in future studies in order to more completely describe the tropical wavelike disturbances which were noted. The equatorial boundary in the current model may, however, cause unreasonable results at lower latitudes than 6.1°N. The model is presently not suitable for use for further study of the eastern boundary disturbances because of grid size limitations. However, a careful study of these features using a higher resolution model having a realistic coastline configuration may be valuable in light of the recent findings of Enfield and Allen (1978).

The present model has little or no synoptic "noise". It is recognized that this feature may be altered if finer resolution or synoptic wind forcing were introduced.

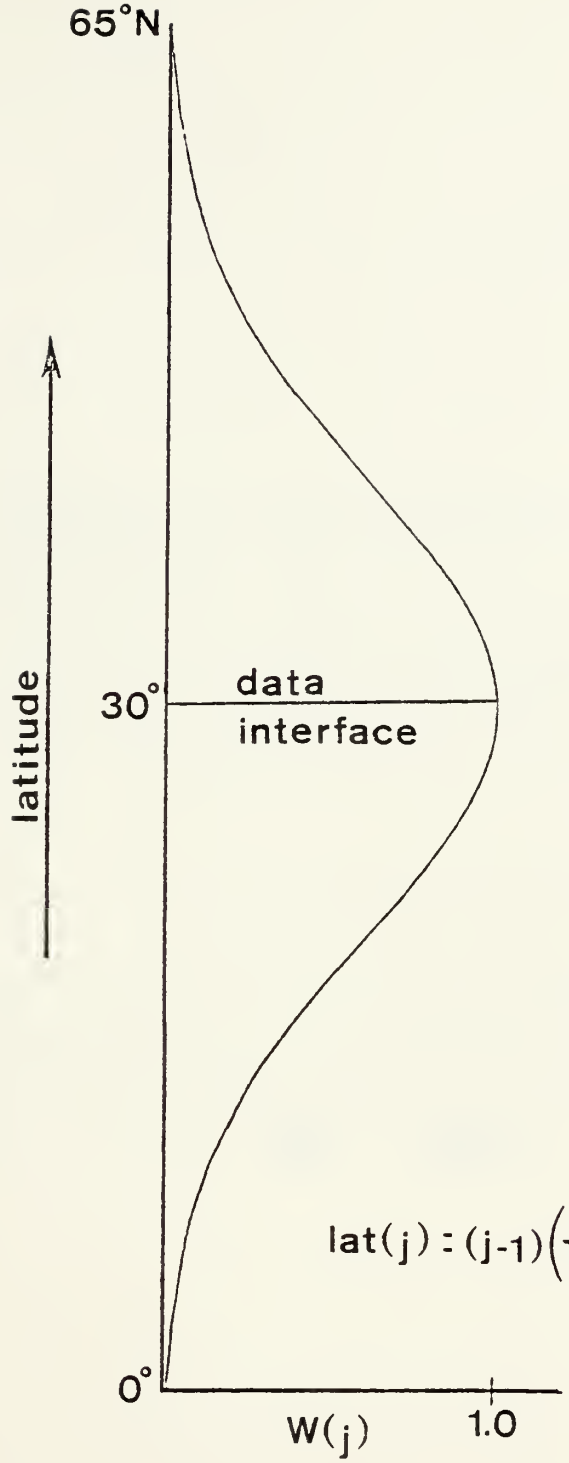


$$lat(j) : (j-1)\left(\frac{65\,\Pi}{180}/32\right),\quad j:1,33$$

$$W(j) : \exp\left\{-\left(\frac{lat(j)\cdot 180}{10\ \Pi} - 3\right)^2 / 2\right\}$$

Figure 1

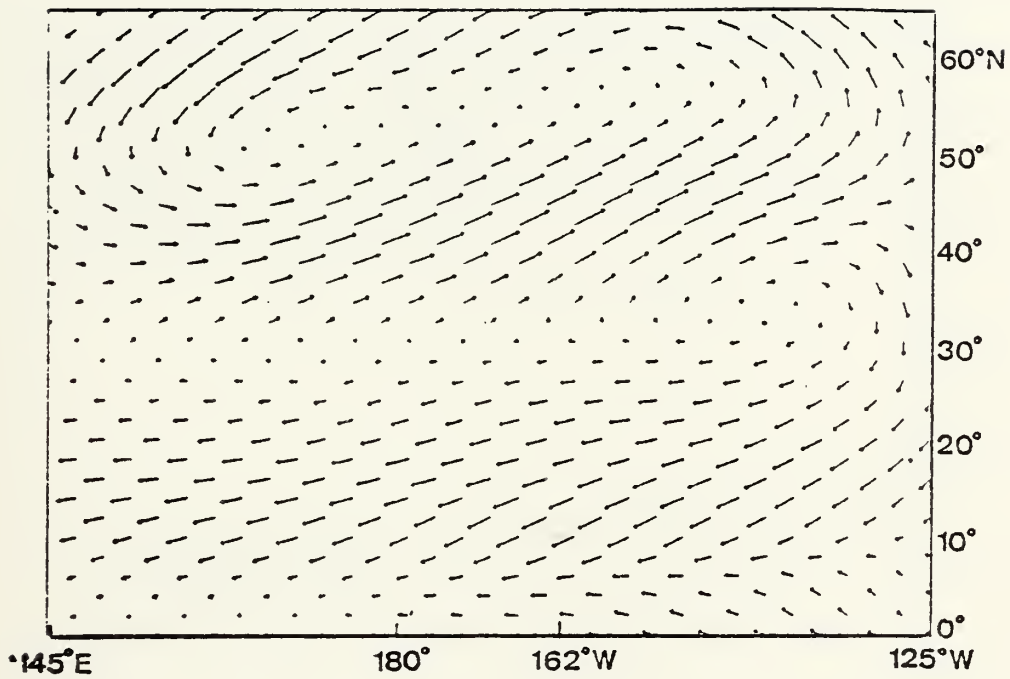


Figure 2

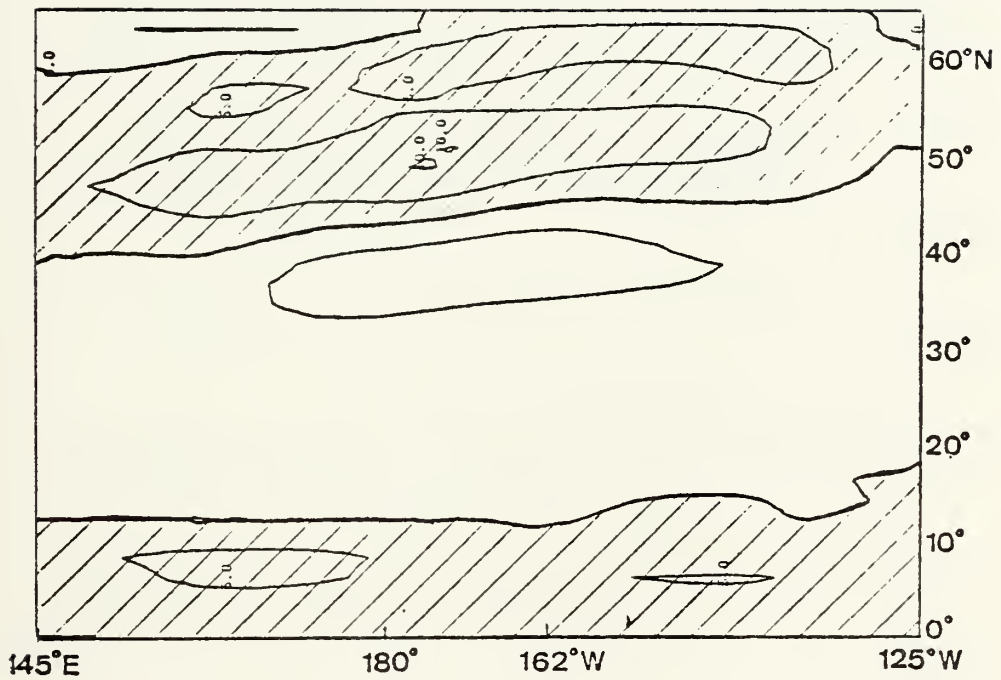


Figure 3

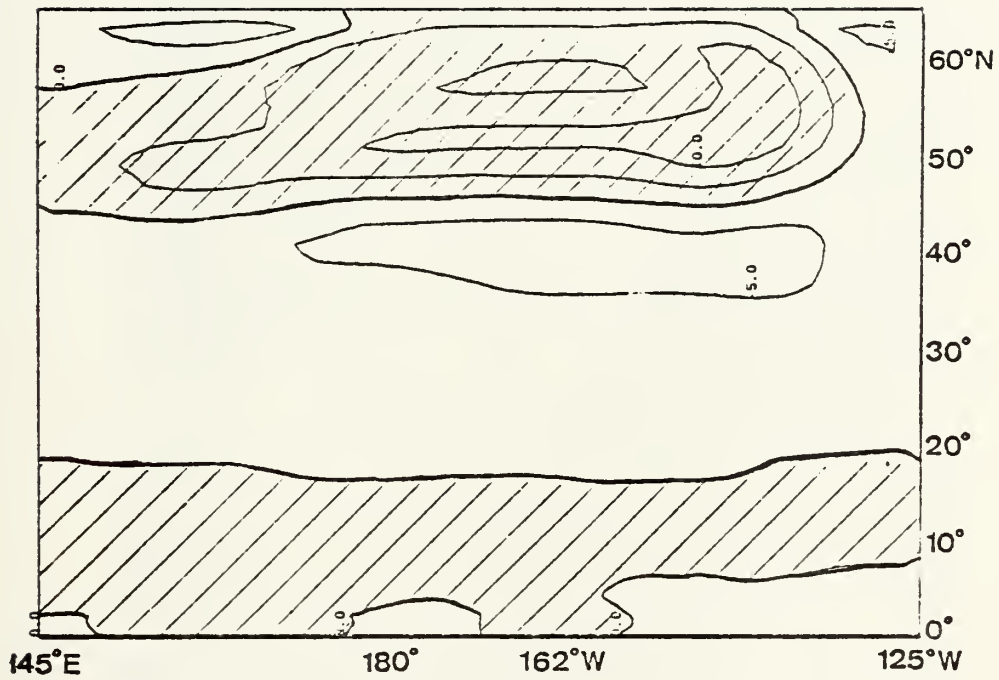


Figure 4

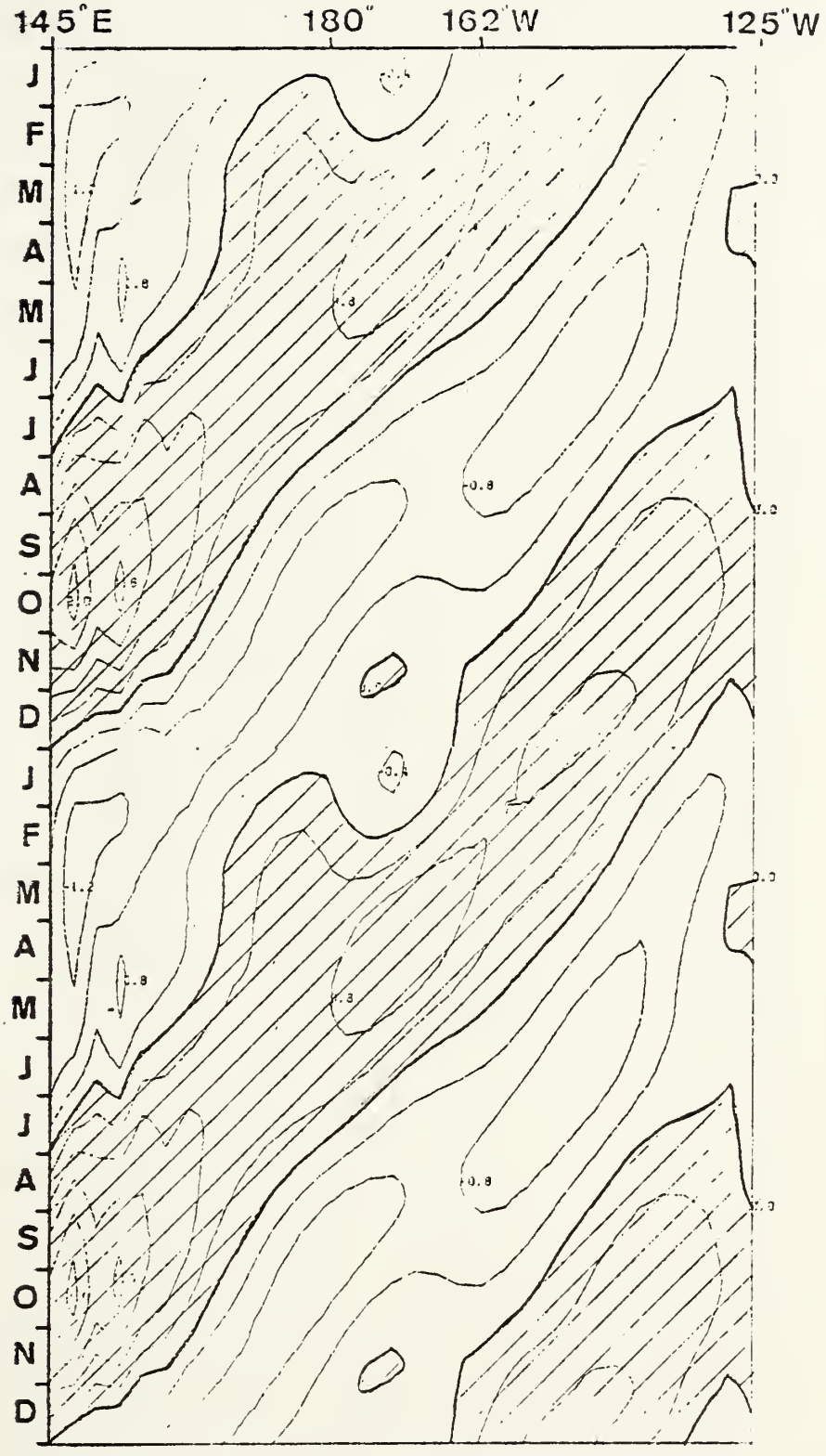


Figure 5

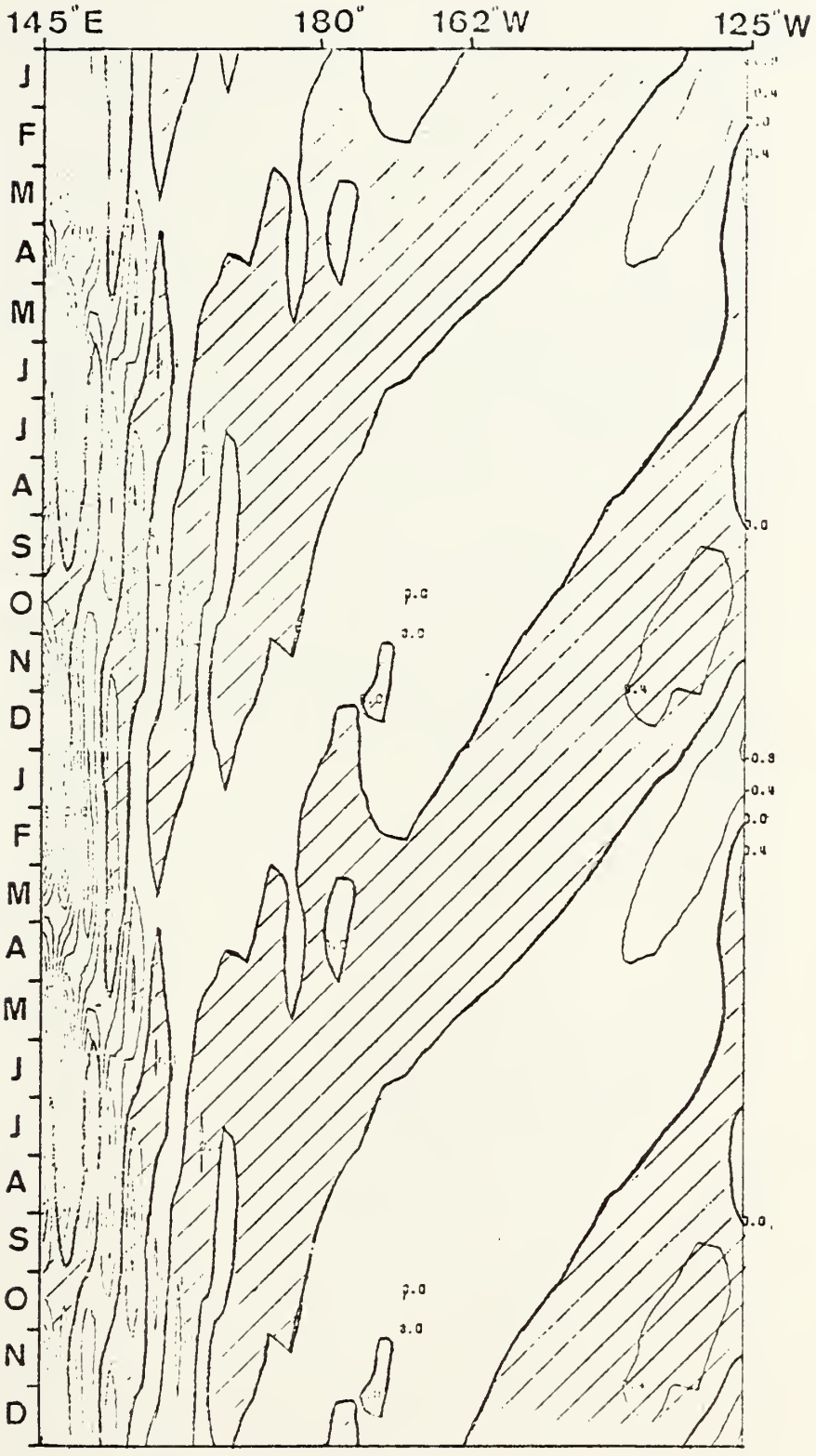


Figure 6

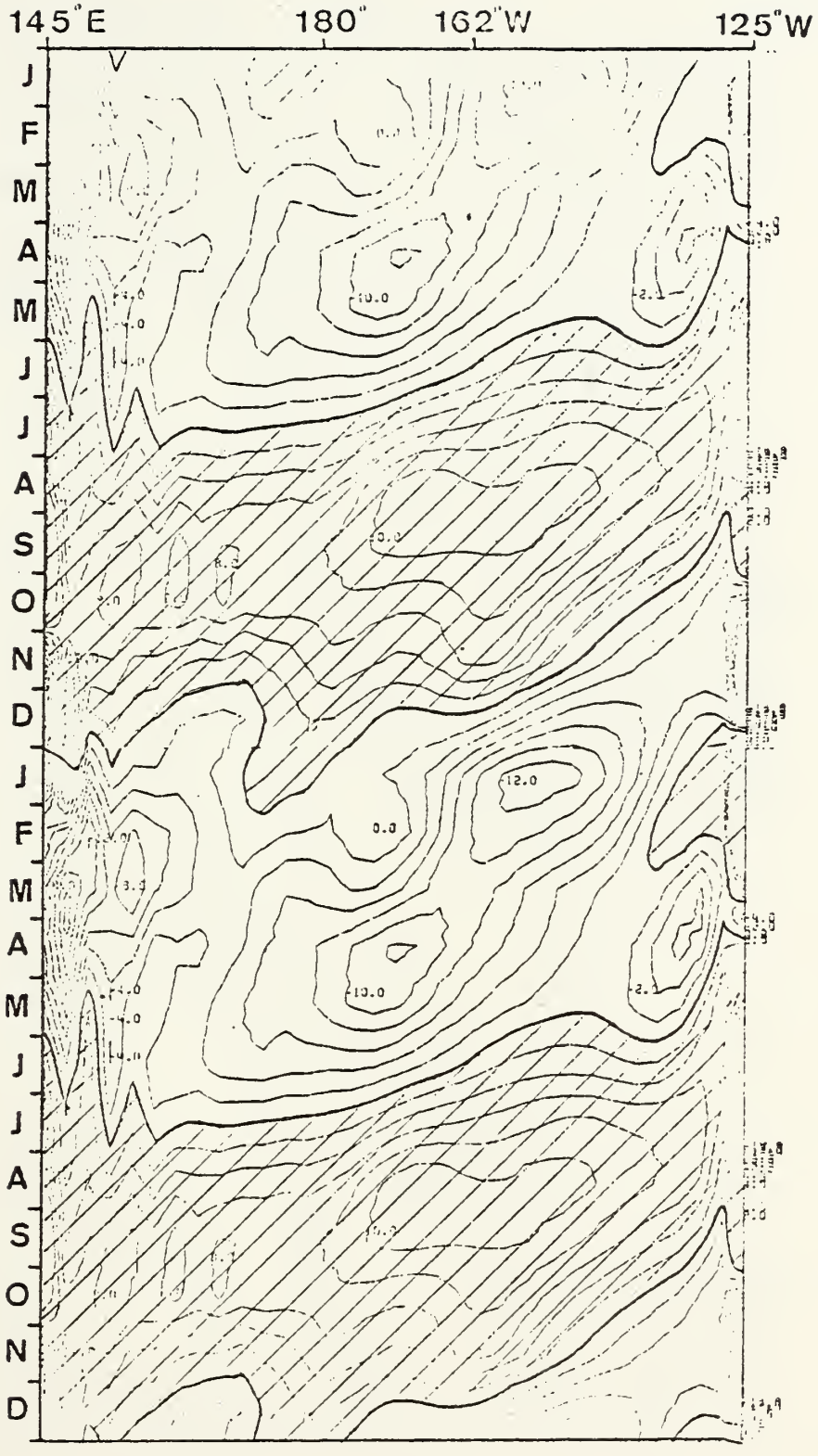
145°E
180°
162°W
125°W
J
F
M
A
M
J
J
A
S
O
N
D
J
F
M
A
M
J
J
A
S
O
N
D
10.0
12.0
0.0
10.0

Figure 7

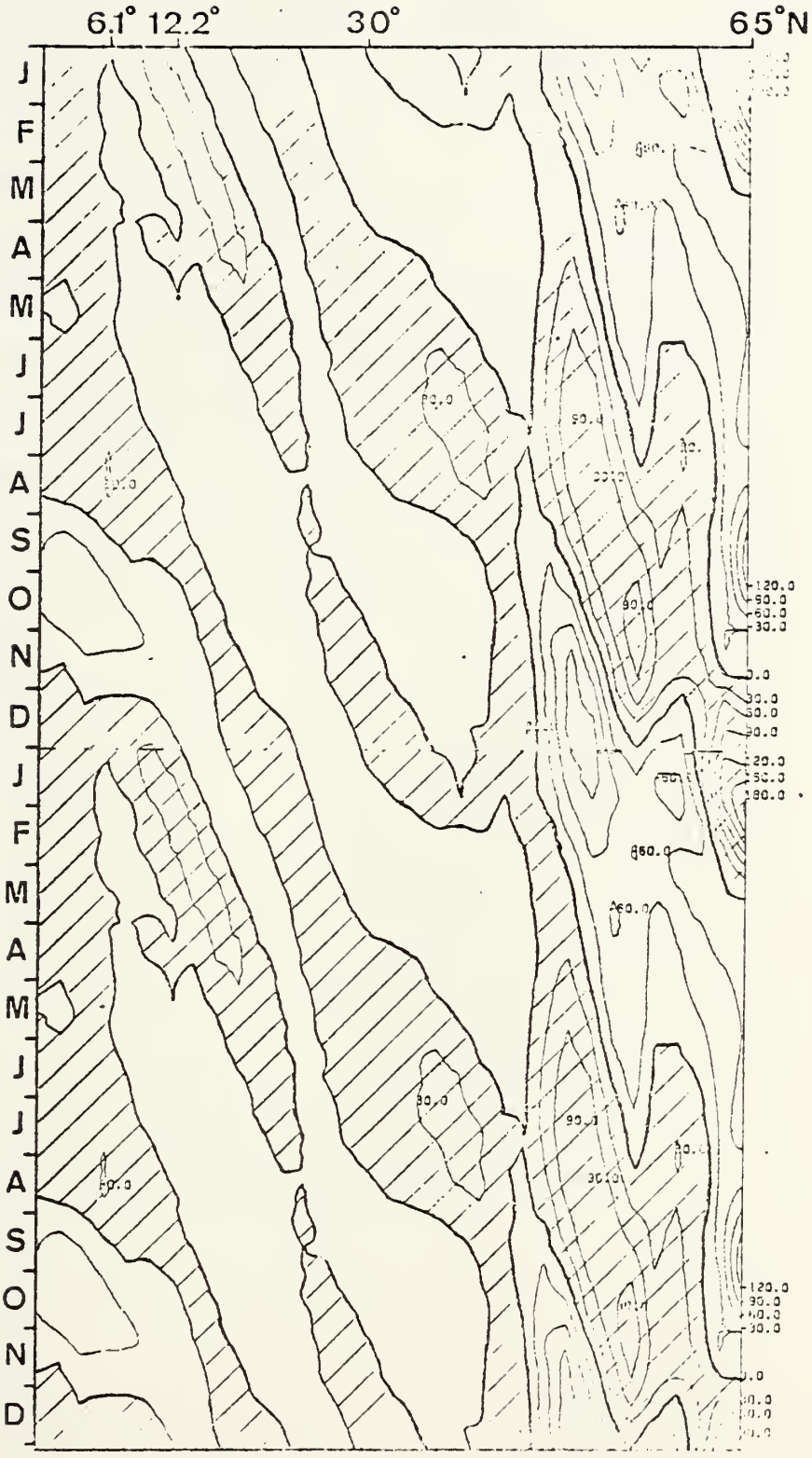


Figure 8

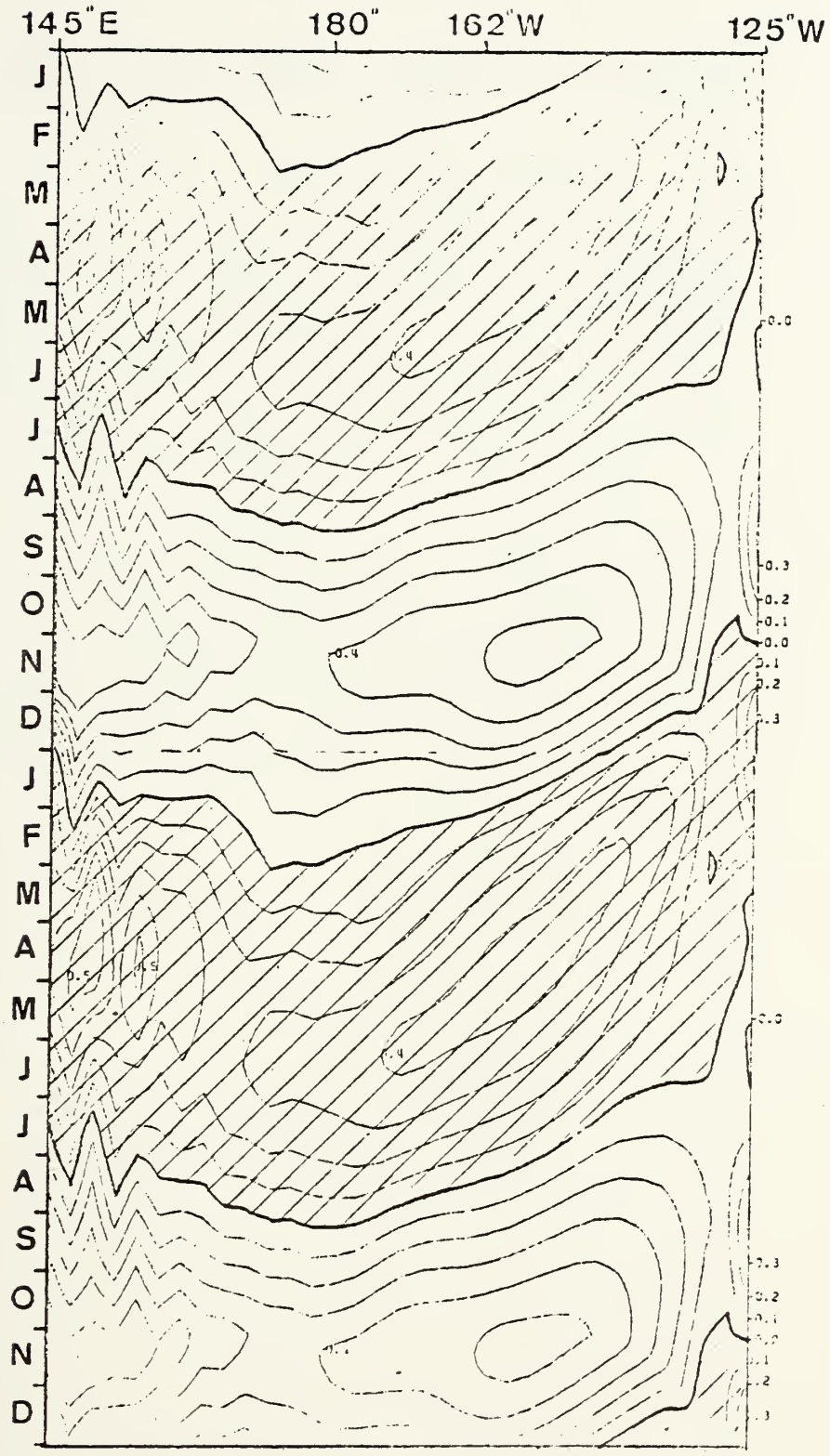
145°E
180°
162°W
125°W
J
F
M
A
M
J
J
A
S
O
N
D
J
F
M
A
M
J
J
A
S
O
N
D
0.0
0.3
0.2
0.1
0.0
0.1
0.2
0.3
0.0
0.3
0.2
0.1
0.2
0.3

Figure 9

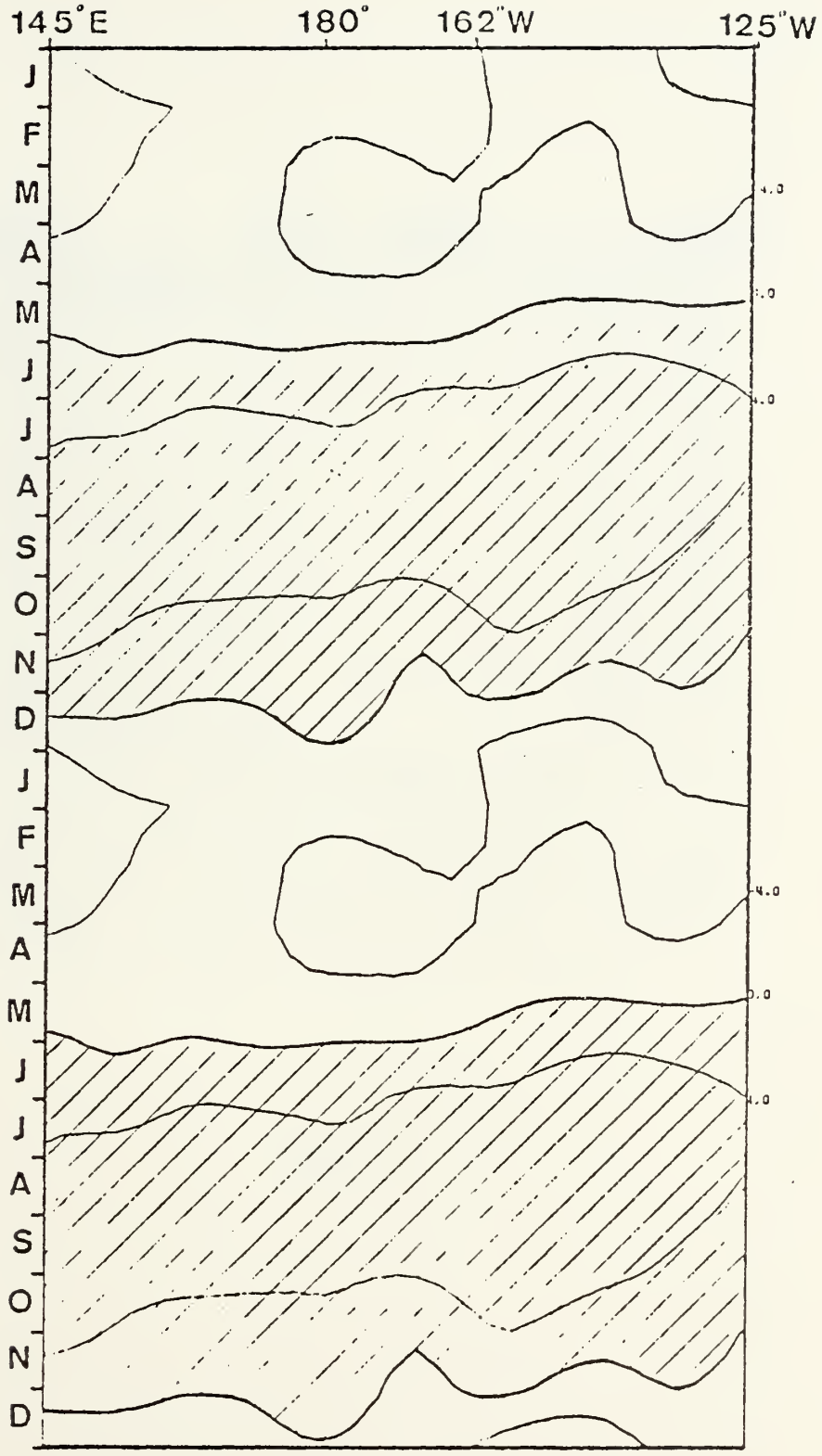


Figure 10

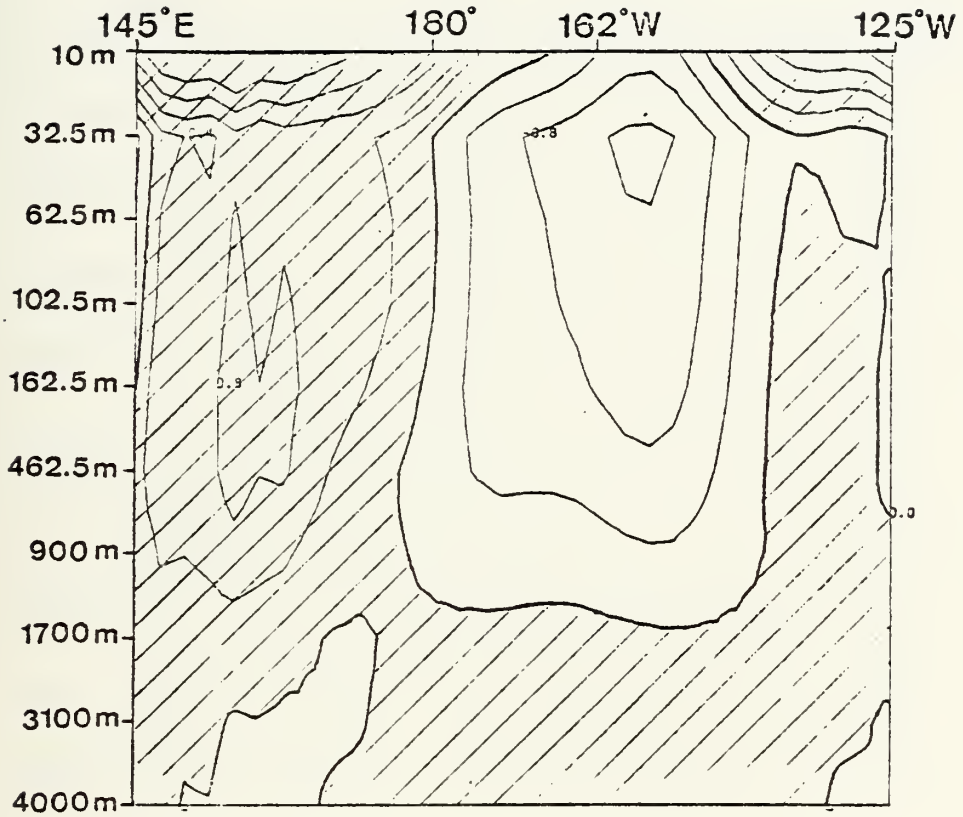
145°E
180°
162°W
125°W
10 m
32.5 m
62.5 m
102.5 m
162.5 m
462.5 m
900 m
1700 m
3100 m
4000 m

Figure 11

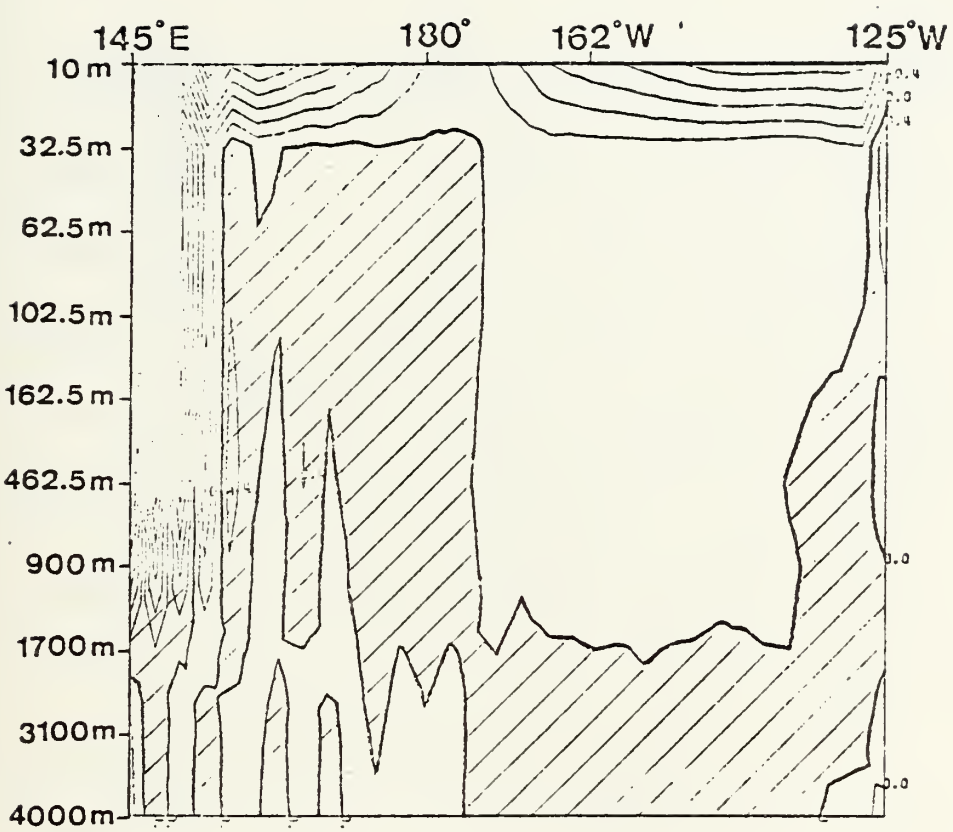
145°E
180°
162°W
125°W
10 m
32.5 m
62.5 m
102.5 m
162.5 m
462.5 m
900 m
1700 m
3100 m
4000 m

Figure 12

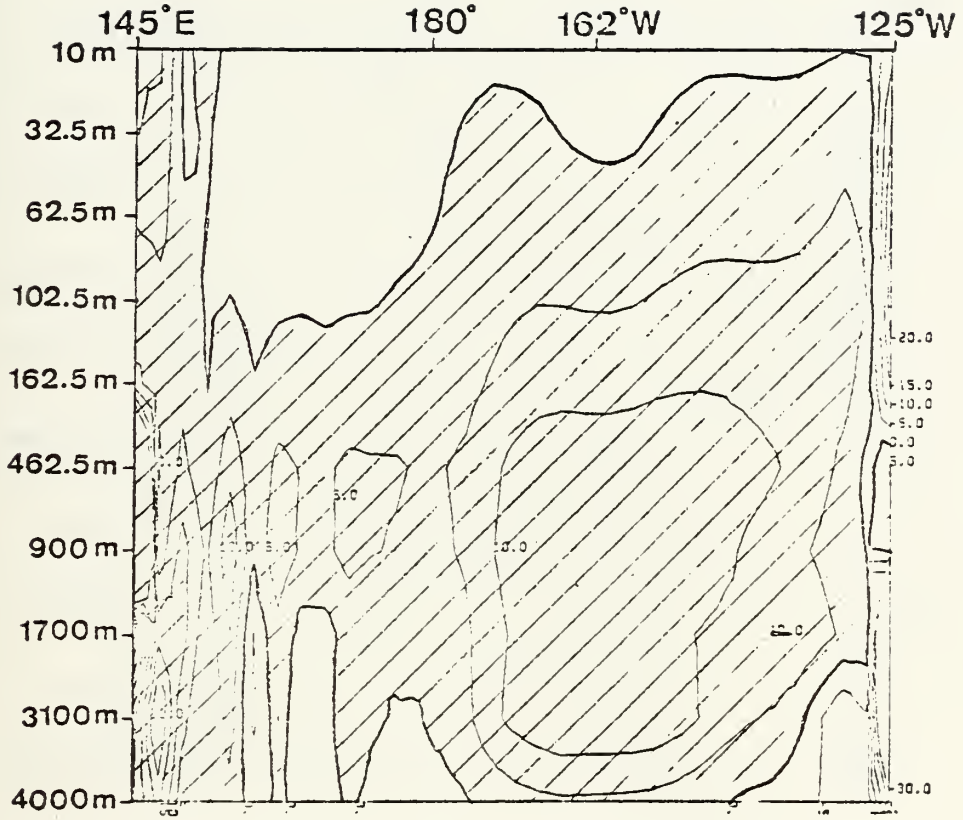
145°E
180°
162°W
125°W
10 m
32.5 m
62.5 m
102.5 m
162.5 m
462.5 m
900 m
1700 m
3100 m
4000 m

Figure 13

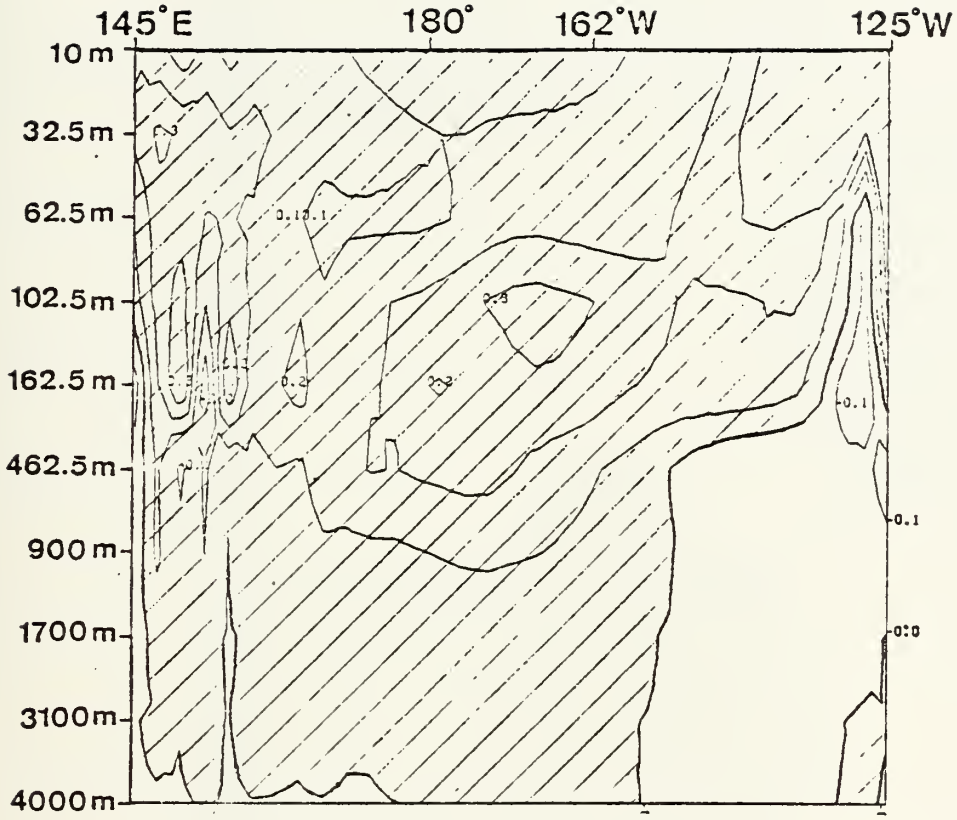
145°E
180°
162°W
125°W
10 m
32.5 m
62.5 m
102.5 m
162.5 m
462.5 m
900 m
1700 m
3100 m
4000 m

Figure 14

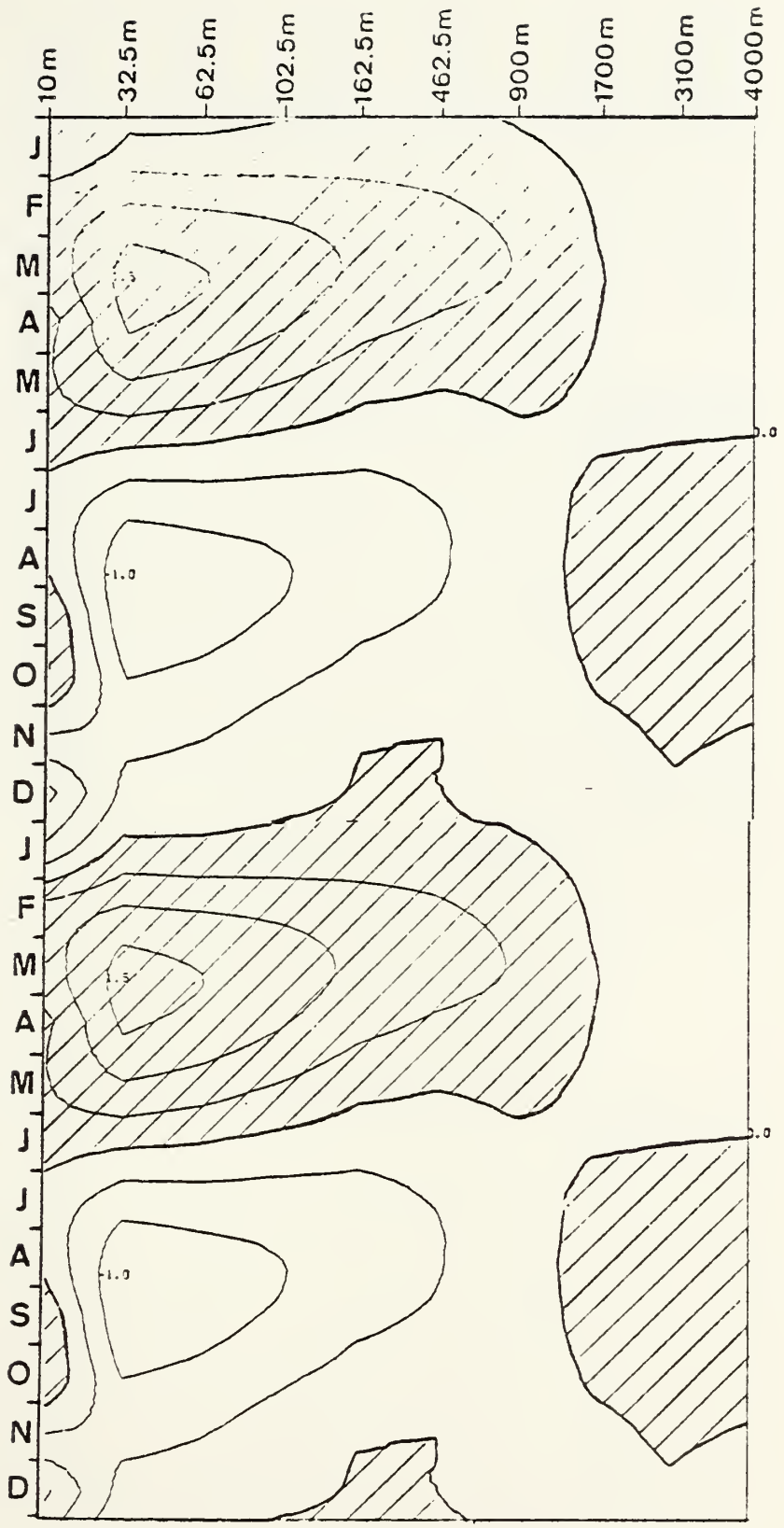
10m
32.5m
62.5m
102.5m
162.5m
462.5m
900m
1700m
3100m
4000m
J
F
M
A
M
J
J
A
S
O
N
D
J
F
M
A
M
J
J
A
S
O
N
D
-1.0
-1.0

Figure 15

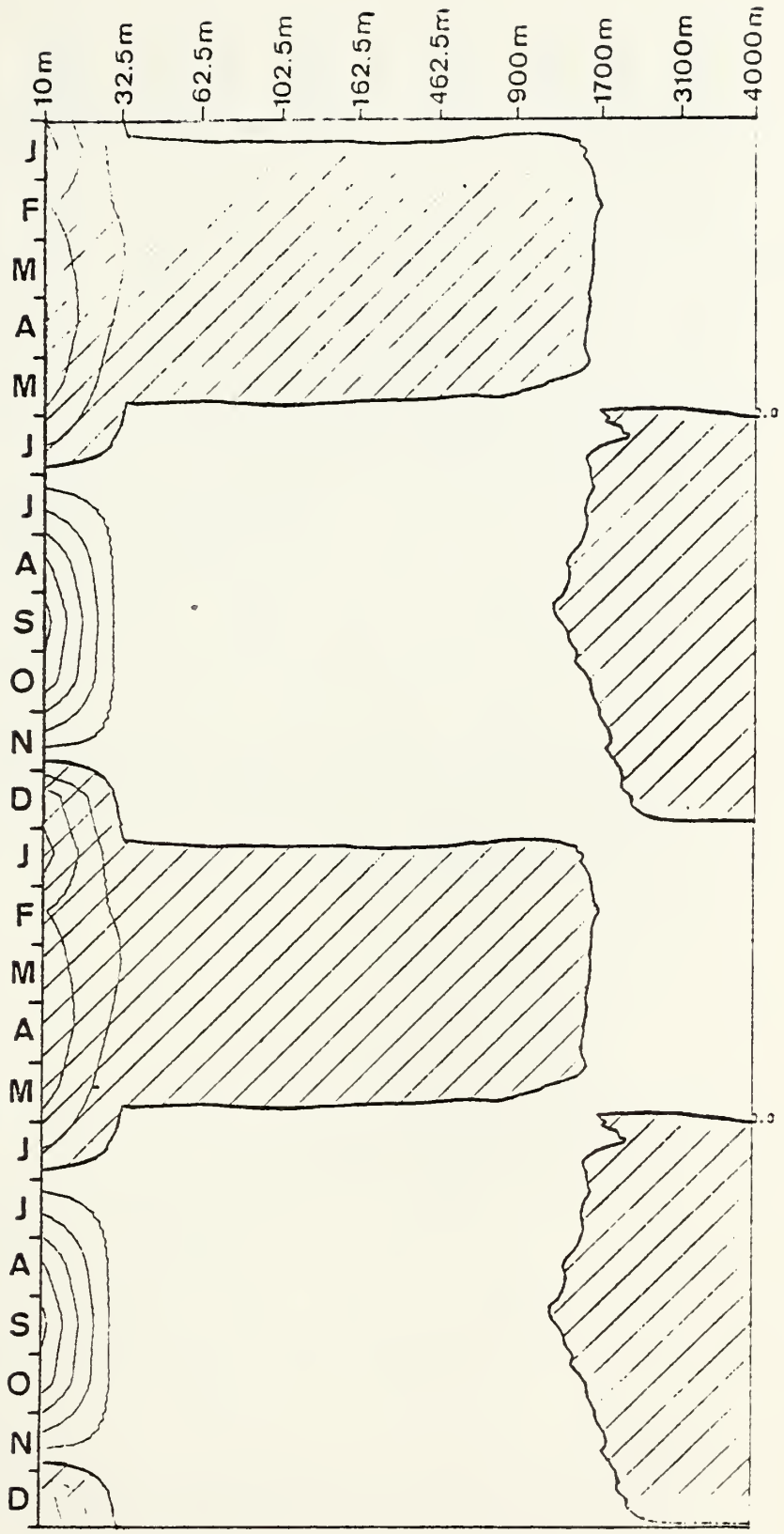
10m
32.5m
62.5m
102.5m
162.5m
462.5m
900m
1700m
3100m
4000m
J
F
M
A
M
J
J
A
S
O
N
D
J
F
M
A
M
J
J
A
S
O
N
D

Figure 16

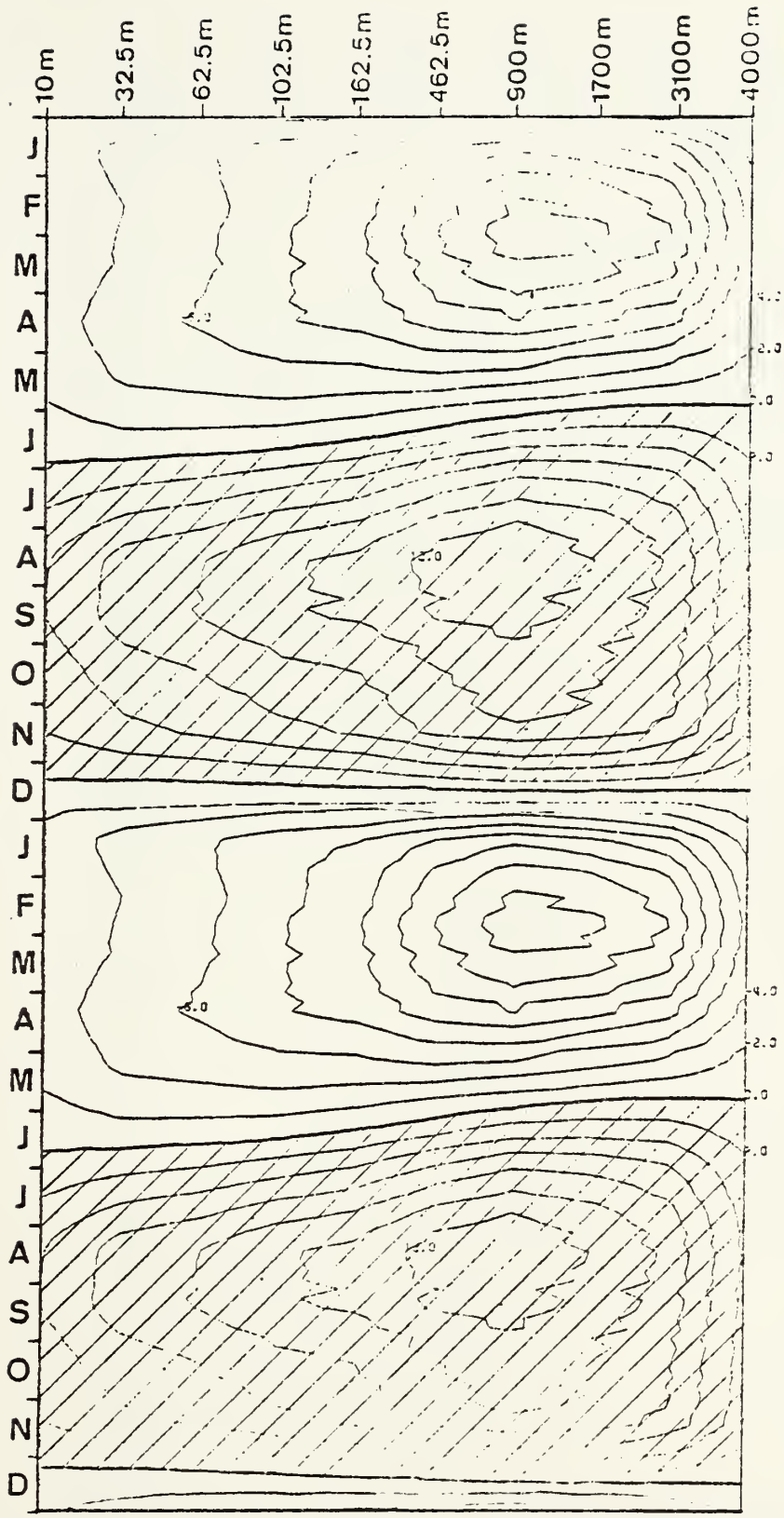
10m
32.5m
62.5m
102.5m
162.5m
462.5m
900m
1700m
3100m
4000m
J
F
M
A
M
J
J
A
S
O
N
D
J
F
M
A
M
J
J
A
S
O
N
D

Figure 17

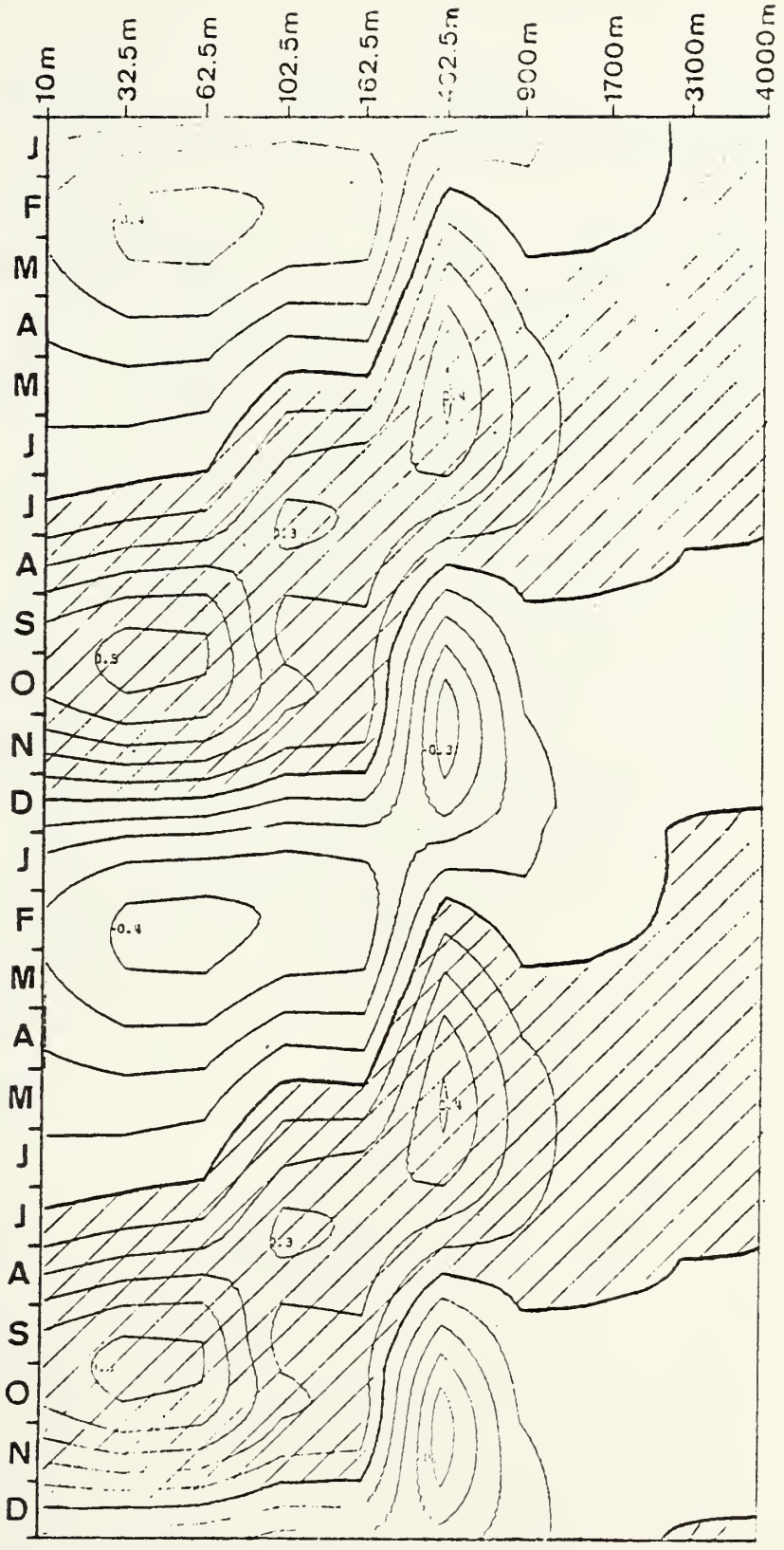
10m
32.5m
62.5m
102.5m
162.5m
900m
1700m
3100m
4000m
J
F
M
A
M
J
J
A
S
O
N
D
J
F
M
A
M
J
J
A
S
O
N
D

Figure 18

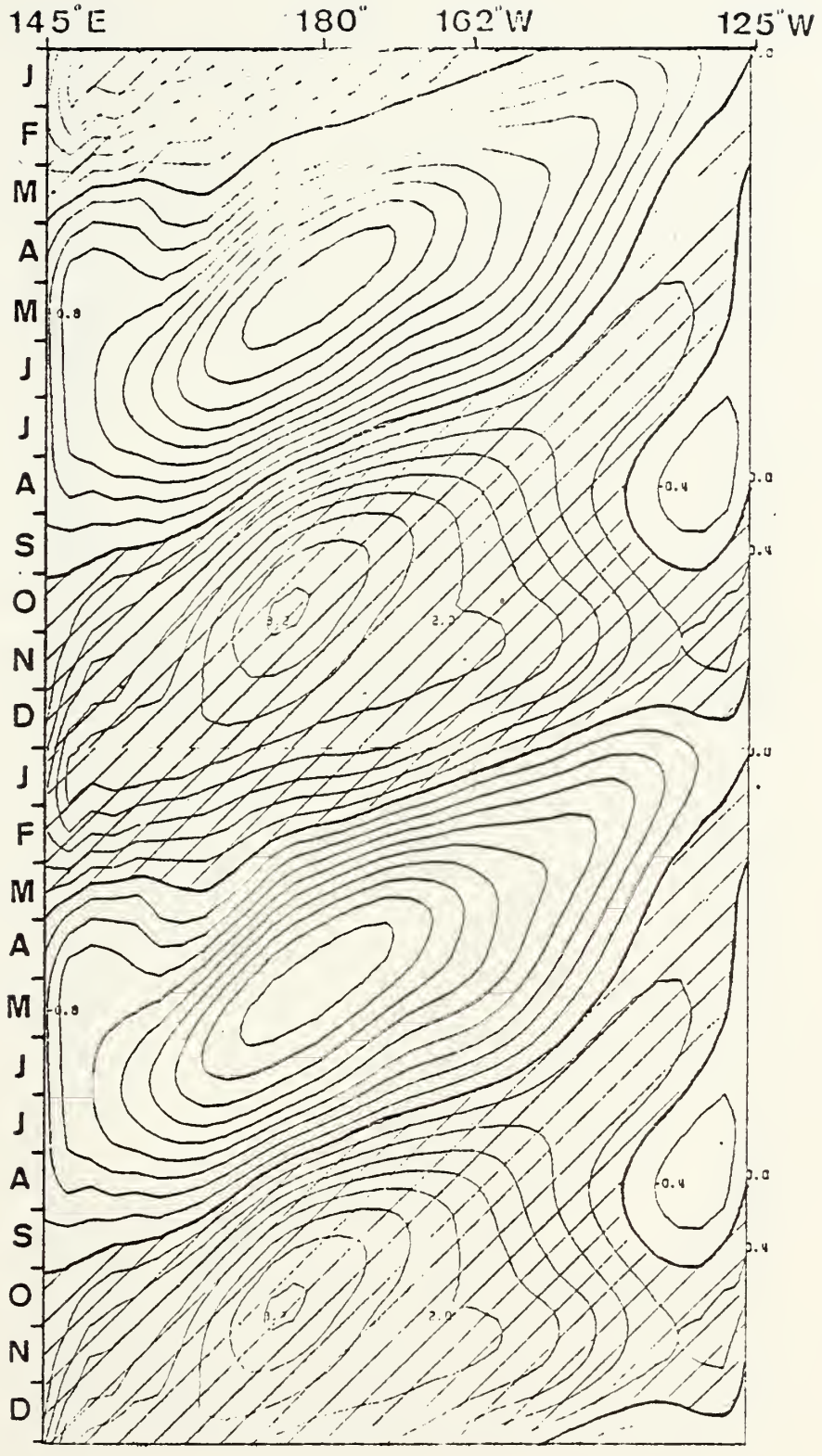


Figure 19

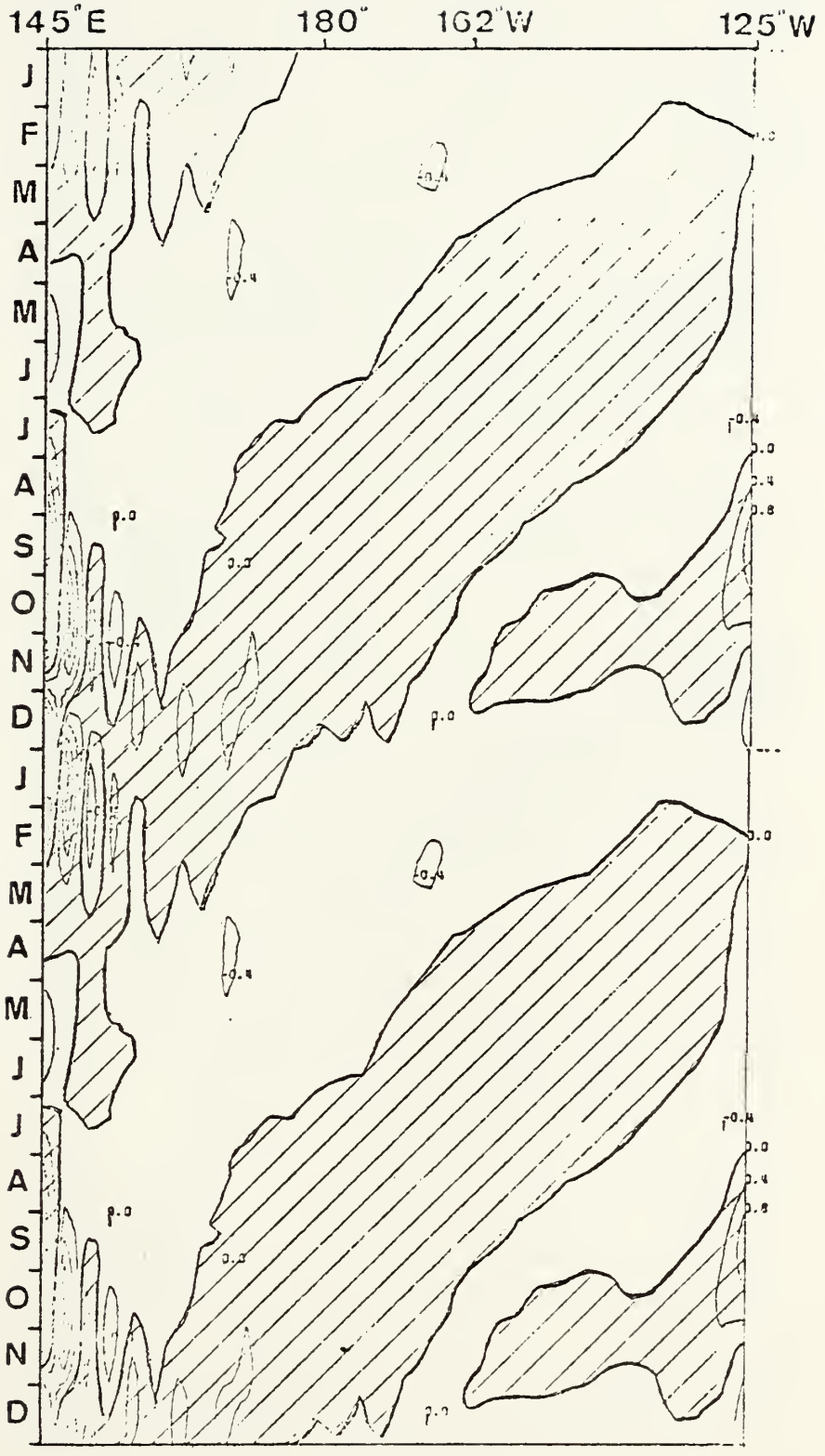


Figure 20

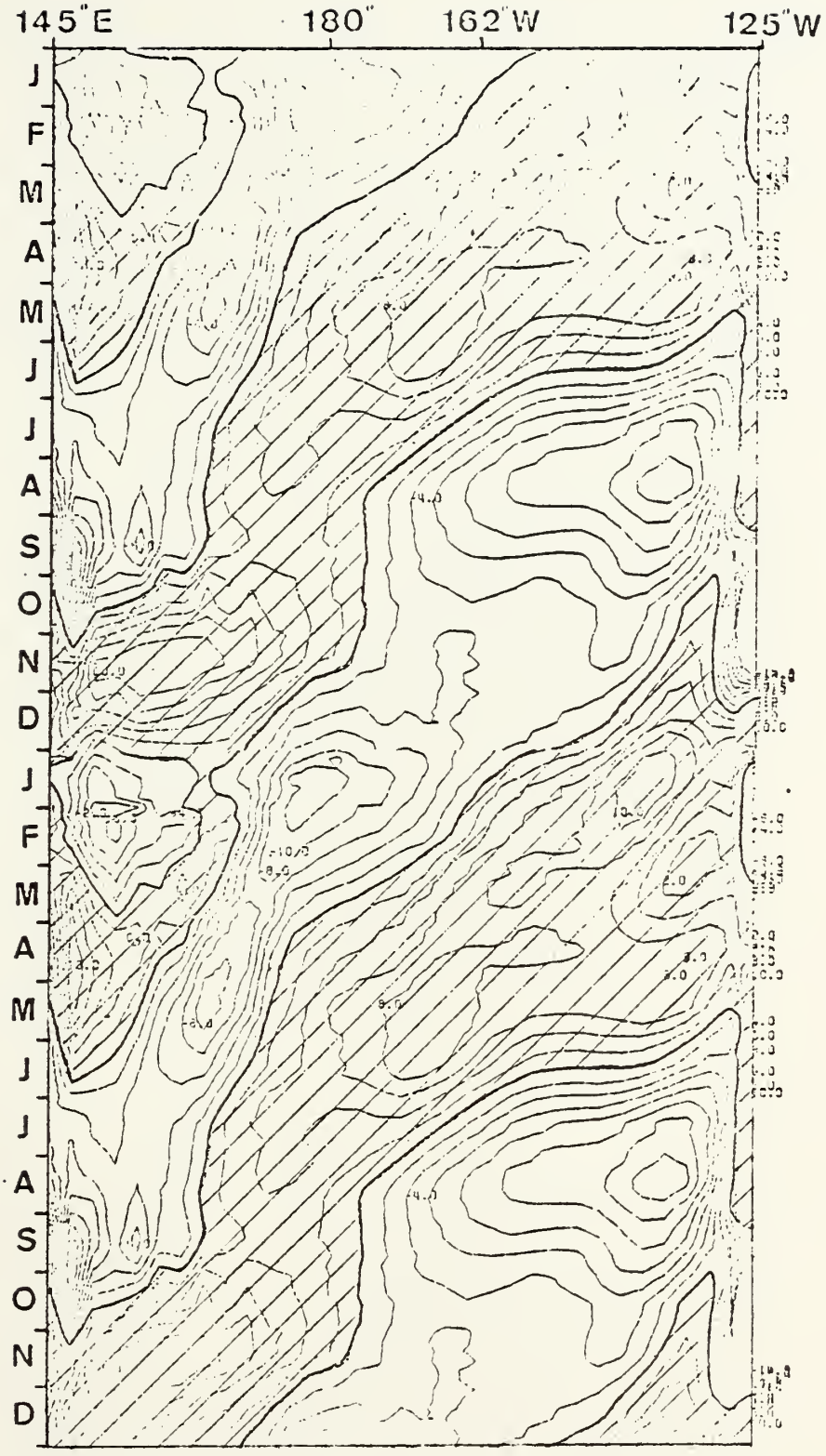


Figure 21

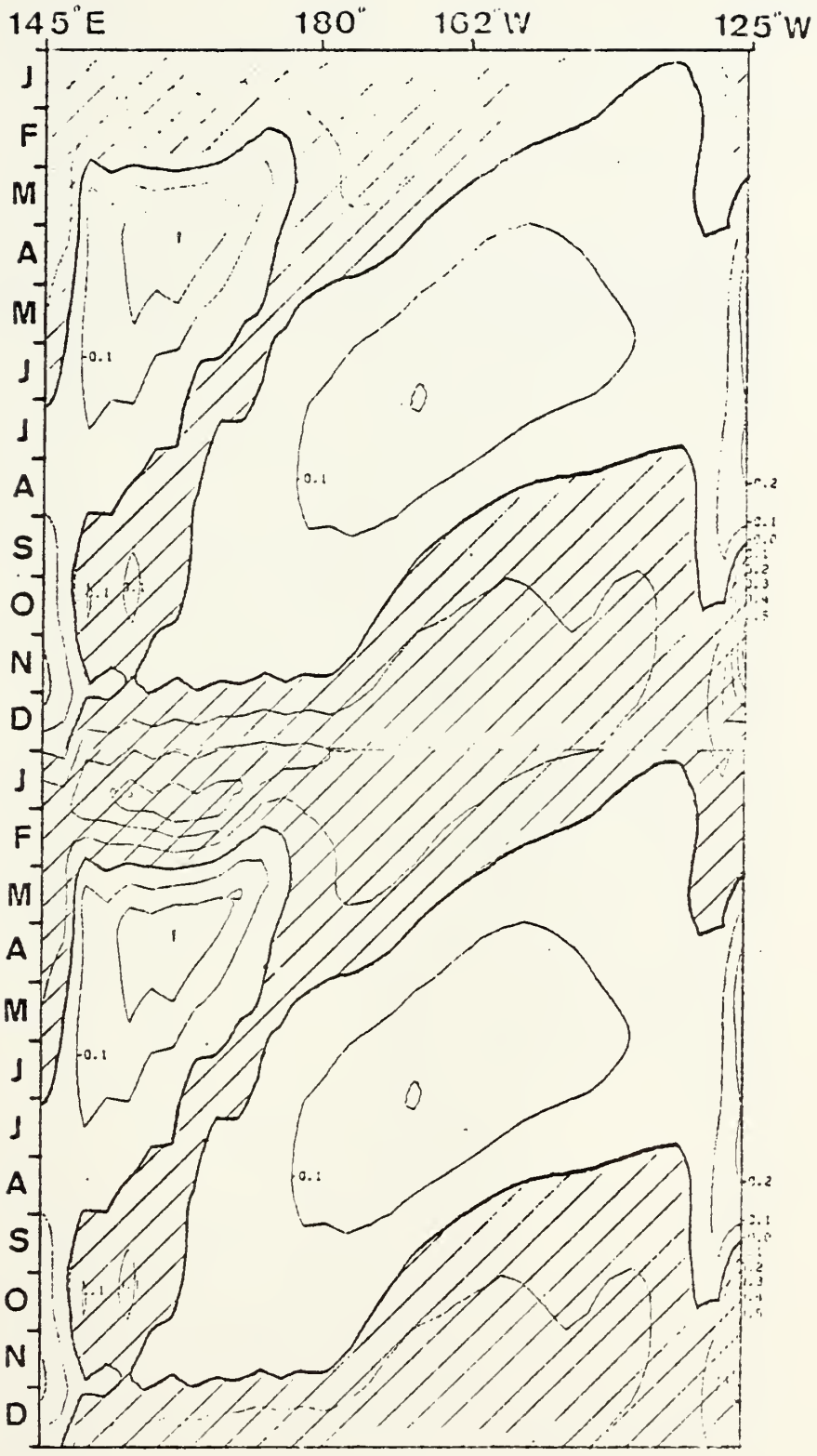
145°E
180°
162°W
125°W
J
F
M
A
M
J
J
A
S
O
N
D
J
F
M
A
M
J
J
A
S
O
N
D
0.1
0.1
0.1
0.1
0.2
0.2

Figure 22

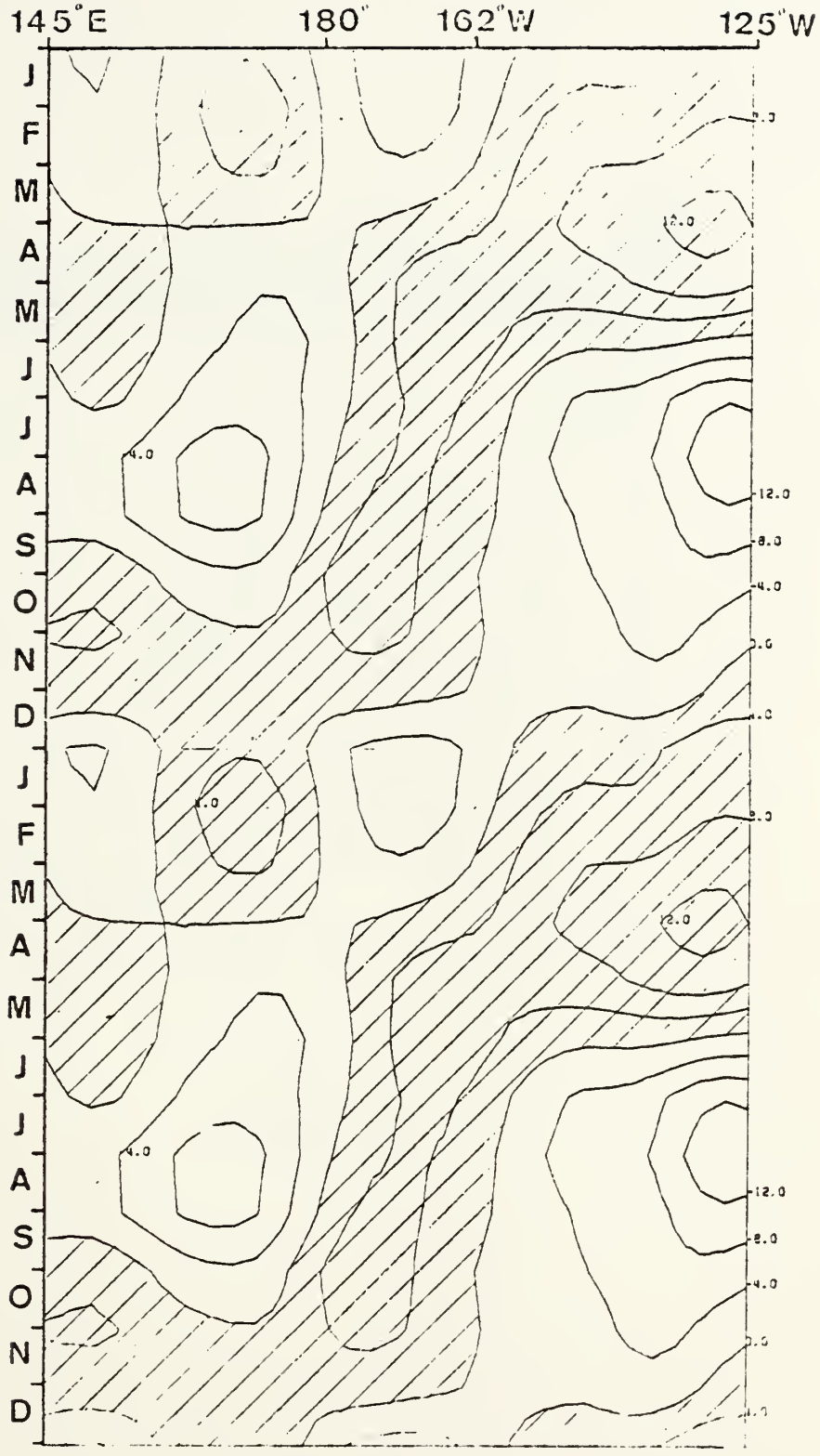
145°E
180°
162°W
125°W
J
F
M
A
M
J
J
A
S
O
N
D
J
F
M
A
M
J
J
A
S
O
N
D
4.0
4.0
4.0
12.0
8.0
4.0
0.0
12.0
8.0
4.0
0.0

Figure 23

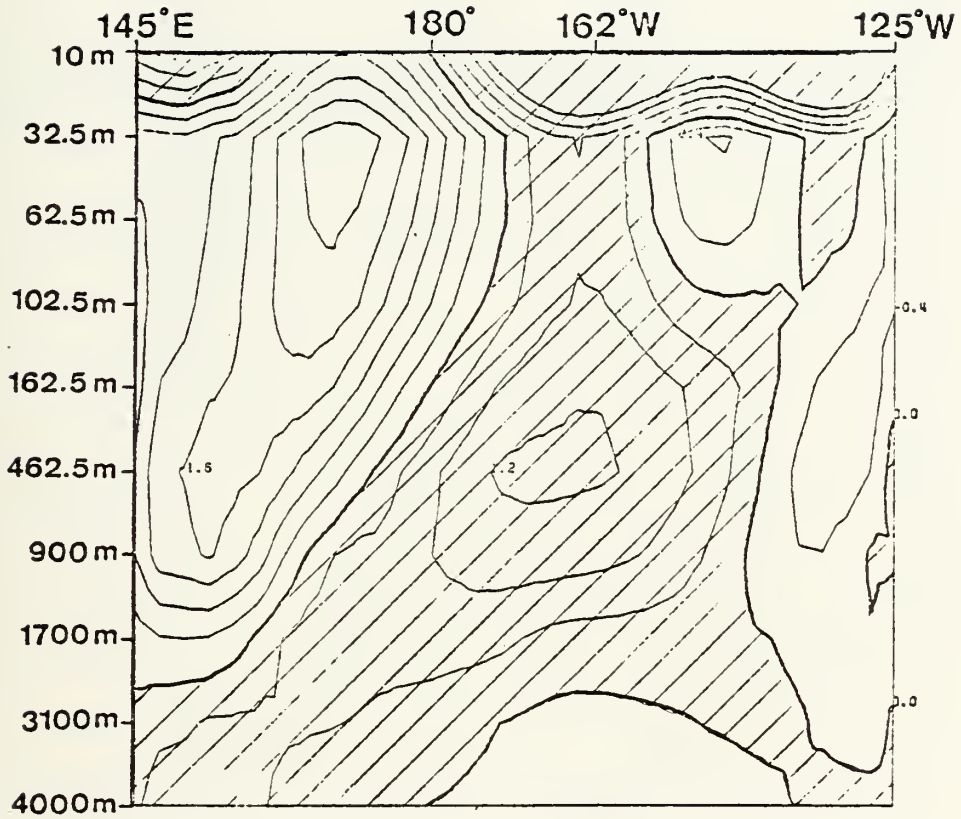
145°E
180°
162°W
125°W
10 m
32.5 m
62.5 m
102.5 m
162.5 m
462.5 m
900 m
1700 m
3100 m
4000 m
1.5
.2
0.4
1.0
3.0

Figure 24

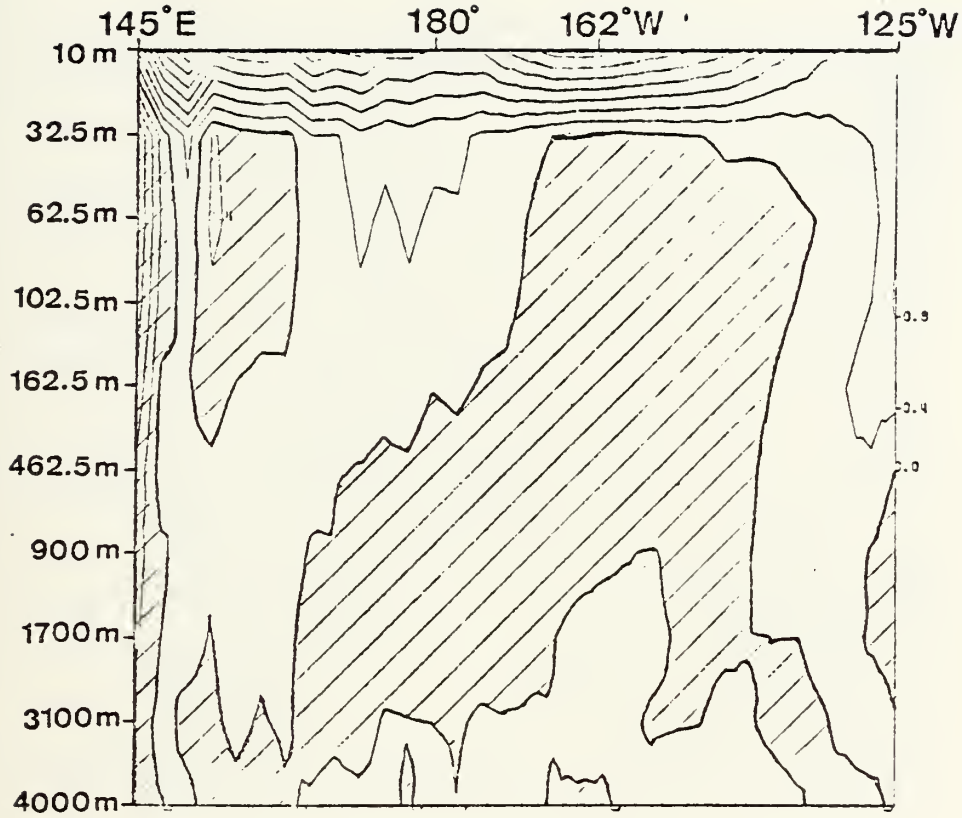
145°E
180°
162°W
125°W
10 m
32.5 m
62.5 m
102.5 m
162.5 m
462.5 m
900 m
1700 m
3100 m
4000 m

Figure 25

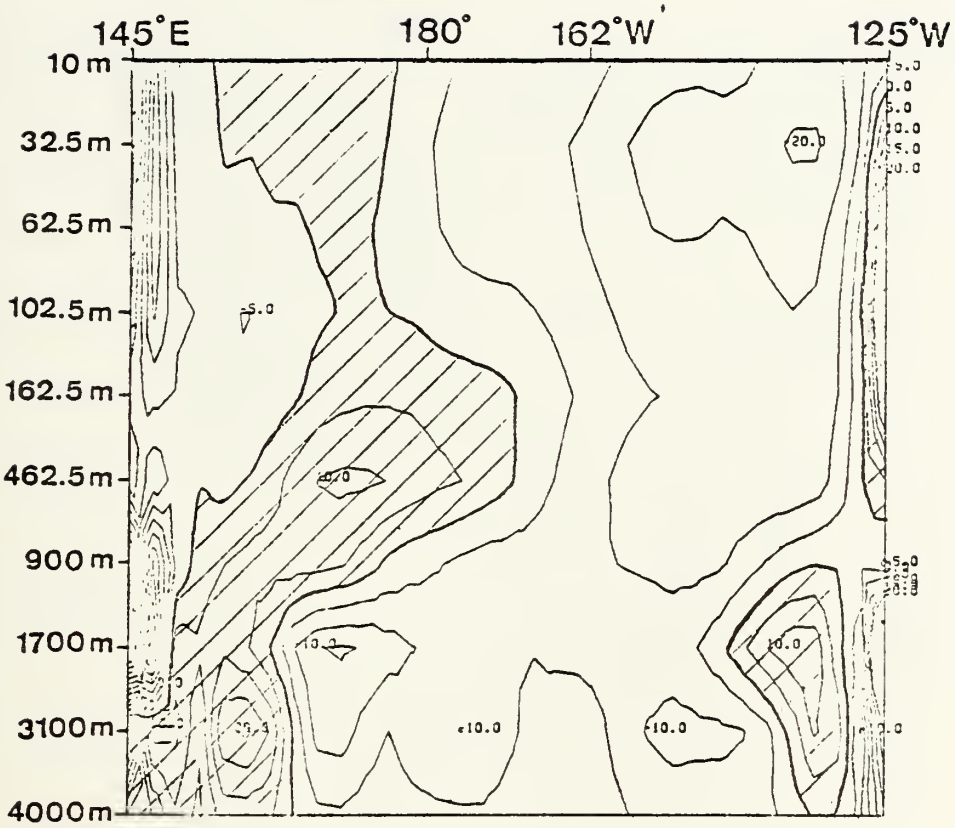
145°E
180°
162°W
125°W
10 m
32.5 m
62.5 m
102.5 m
162.5 m
462.5 m
900 m
1700 m
3100 m
4000 m
20.0
10.0
10.0

Figure 26

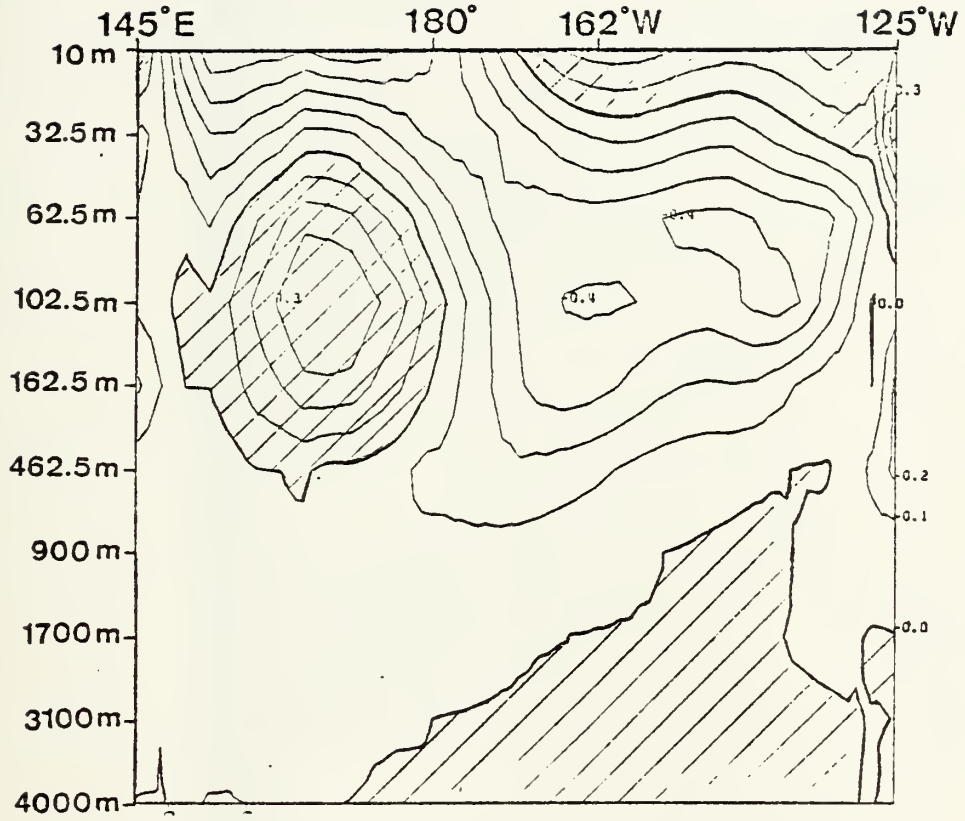
145°E
180°
162°W
125°W
10 m
32.5 m
62.5 m
102.5 m
162.5 m
462.5 m
900 m
1700 m
3100 m
4000 m
0.3
0.4
0.0
0.2
0.1
0.0

Figure 27

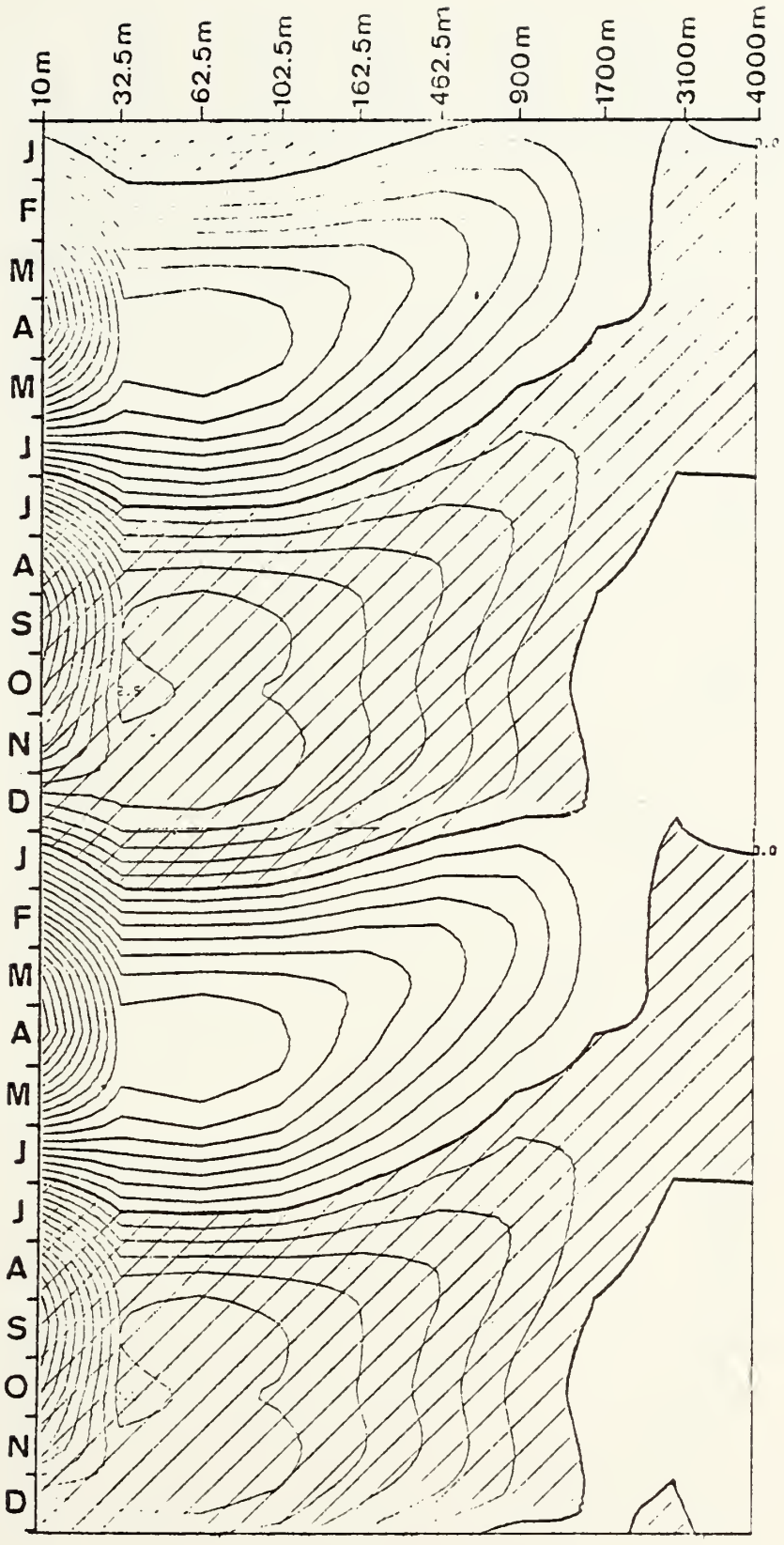
10m
32.5m
62.5m
102.5m
162.5m
462.5m
900m
1700m
3100m
4000m
J
F
M
A
M
J
J
A
S
O
N
D
J
F
M
A
M
J
J
A
S
O
N
D

Figure 28

10m
32.5m
62.5m
102.5m
162.5m
462.5m
900m
1700m
3100m
4000m
J
F
M
A
M
J
J
A
S
O
N
D
J
F
M
A
M
J
J
A
S
O
N
D
-0.5
-0.5
0.0
0.0
0.0

Figure 29

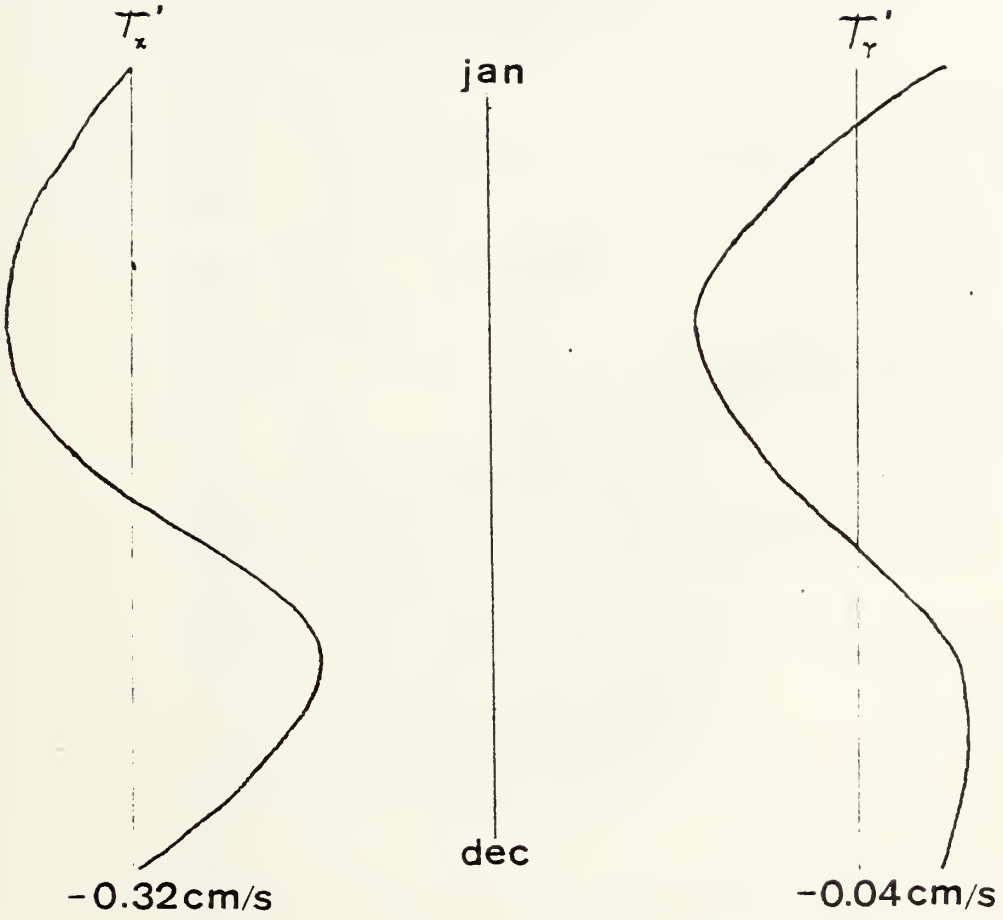


Figure 30

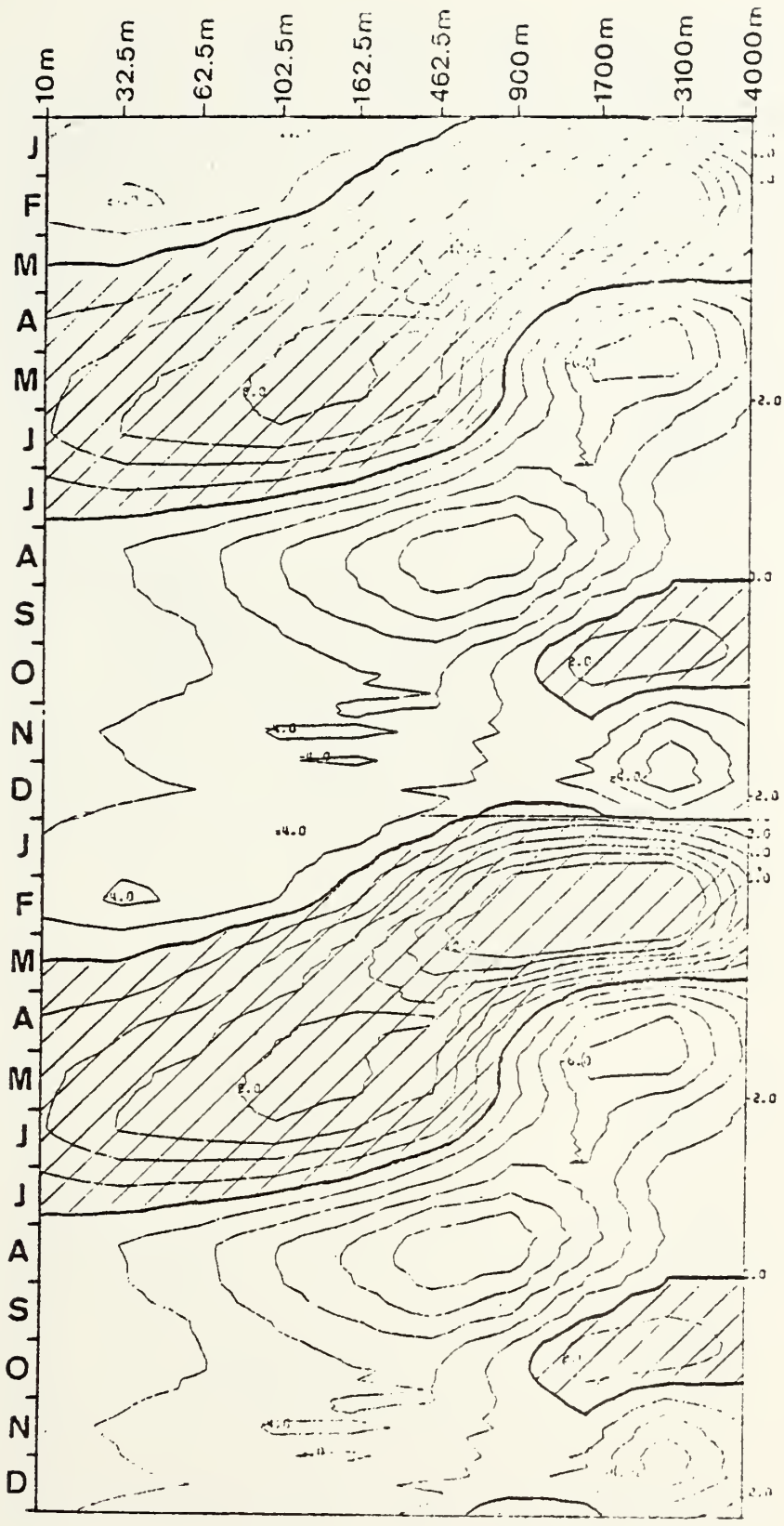
10m
32.5m
62.5m
102.5m
162.5m
462.5m
900m
1700m
3100m
4000m
J
F
M
A
M
J
J
A
S
O
N
D
J
F
M
A
M
J
J
A
S
O
N
D
2.0
4.0

Figure 31

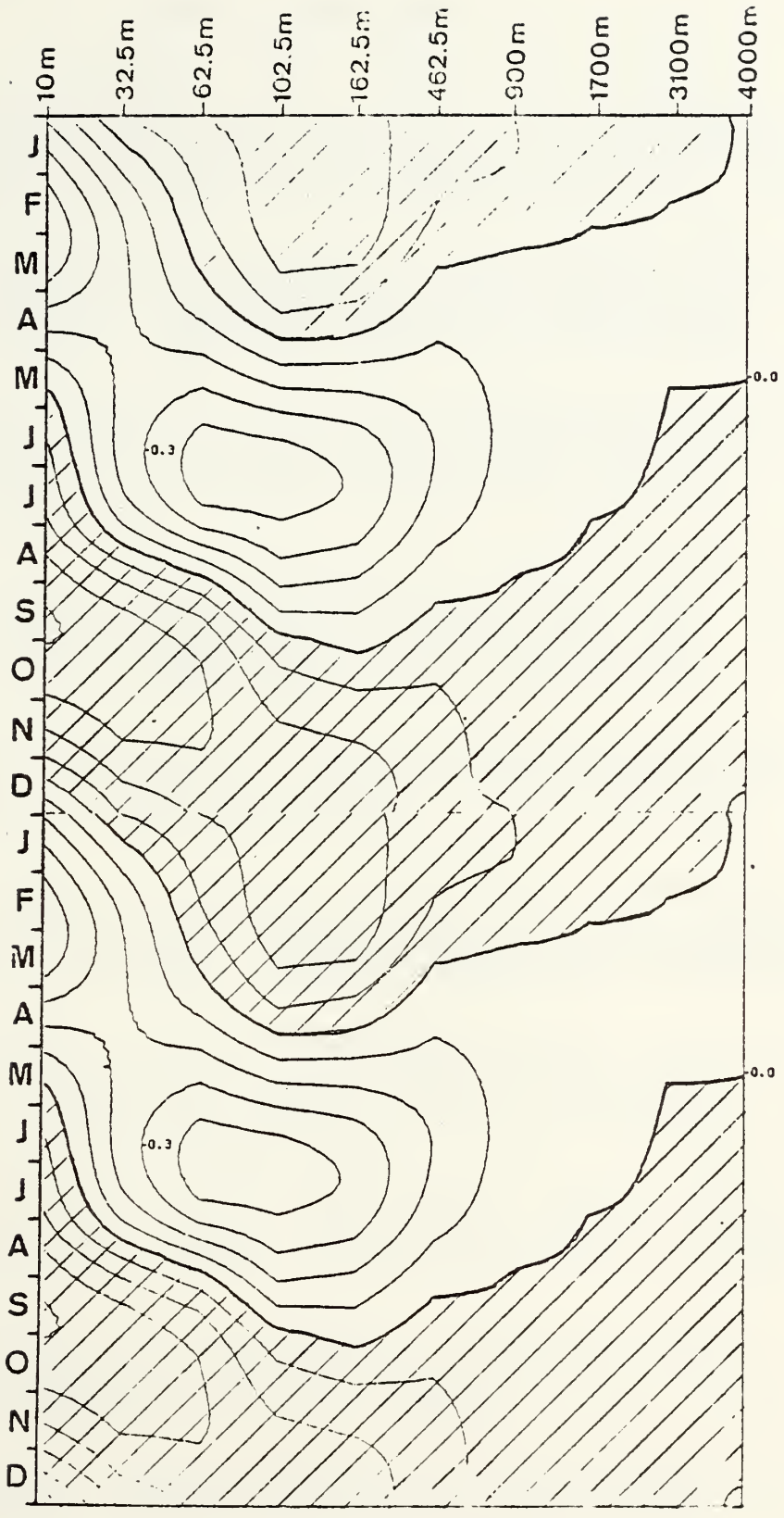
10m
32.5m
62.5m
102.5m
162.5m
462.5m
900m
1700m
3100m
4000m
J
F
M
A
M
J
J
A
S
O
N
D
J
F
M
A
M
J
J
A
S
O
N
D
-0.3
-0.3
0.0
0.0

Figure 32

# LIST OF REFERENCES


Businger, J. A., Wyngaard, J. C., Izumi, Y. and Bradley, E. F., "Flux-profile relationships in the atmospheric surface layer", Journal of Atmospheric Sciences, v. 28, p. 181-189, 1971.

DeWitt, F. Webb and Leetmaa, Ants, "A Simple Ekman-Type Model for Predicting Thermocline Displacement in the Tropical Pacific", Journal of Physical Oceanography, v. 8, p. 811-817, September 1978.

Enfield, D. B. and Allen, J. S., "On the Structure and Dynamics of Monthly Mean Sea Level Anomalies Along the Pacific Coast of North and South America", Paper presented at AGU Fall Annual Meeting, San Francisco, CA, December 4-8, 1978.

Haney, Robert L., "A Numerical Study of the Response of an Idealized Ocean to Large-Scale Surface Heat and Momentum Flux", Journal of Physical Oceanography, v. 4, n. 2, p. 145-167, April 1974.

_____, and Davies, R. W., "The Role of Surface Mixing in the Seasonal Variation of the Ocean Thermal Structure", Journal of Physical Oceanography, v. 6, p. 504-510, July 1976.

_____, Shiver, Wayne S. and Hunt, Kenneth H., "A Dynamical-Numerical Study of the Formation and Evolution of Large-Scale Ocean Anomalies", Journal of Physical Oceanography, v. 8, n. 2, p. 952-969, November 1978.

_____, and Wright, J., "The Relationship Between the Grid Size and the Coefficient of Nonlinear Lateral Eddy Viscosity in Numerical Ocean Circulation Models", Journal of Computational Physics, v. 19, p. 257-266, 1975.

Jenne, R. L., Crutcher, H. L., van Loon, H. and Taljaard, J. J., An interim note on Southern Hemisphere climatological grid data, 1969a. (Available from R. L. Jenne, NCAR, Boulder, CO.)

_____, _____ and _____, A selected climatology of the southern hemisphere: computer methods and data availability. NCAR-TN/STR-92, 91 pp, 1969b.

Meyers, G., "On the Annual Rossby Wave in the Tropical North Pacific Ocean", Journal of Physical Oceanography, in review, 1978.

White, W. B., "Annual forcing of baroclinic Rossby waves in the tropical North Pacific", Journal of Physical Oceanography, v. 7, p. 50-61, 1977.

Wunsch, Carl, "Response of an Equatorial Ocean to a Periodic Monsoon", Journal of Physical Oceanography, v. 7, n. 4, p. 497-511, July 1977.

Wyrtki, K., "El Nino - The dynamic response of the equatorial Pacific Ocean to atmospheric forcing", Journal of Physical Oceanography, v. 5, p. 572-584, 1975.

_____ and Meyers, G., "The trade wind field over the Pacific Ocean. Part I. The mean field and the mean annual variation", Hawaii Institute of Geophysics Rep. No. HIG-75-1, 26 pp., 1975.

_____ and _____, "The Trade Wind Field Over the Pacific Ocean", Journal of Applied Meteorology, v. 15, p. 698-704, July 1976.

INITIAL DISTRIBUTION LIST

| | | No. Copies |
|---|---|---|
| 1. | Defense Documentation Center<br>Cameron Station<br>Alexandria, Virginia 22314 | 2 |
| 2. | Library, Code 0142<br>Naval Postgraduate School<br>Monterey, California 93940 | 2 |
| 3. | Dr. G. J. Haltiner, Code 63Ha<br>Department of Meteorology<br>Naval Postgraduate School<br>Monterey, California 93940 | 1 |
| 4. | Dr. R. L. Haney, Code 63Hy<br>Department of Meteorology<br>Naval Postgraduate School<br>Monterey, California 93940 | 2 |
| 5. | LT R. D. LeRoy, USN<br>N.W.S.E.D. Box 81<br>U. S. Naval Air Station<br>FPO San Francisco 96637 | 2 |
| 6. | Dr. C. P. Chang, Code 63Cp<br>Department of Meteorology<br>Naval Postgraduate School<br>Monterey, California 93940 | 1 |
| 7. | Meteorology Department<br>Code 63, Library<br>Naval Postgraduate School<br>Monterey, California 93940 | 1 |
| 8. | Prof. John Allen<br>School of Oceanography<br>Oregon State University<br>Corvallis, Oregon 97331 | 1 |
| 9. | Prof. Lorenz Magaard<br>Department of Oceanography<br>University of Hawaii<br>Honolulu, Hawaii 96822 | 1 |
| 10. | Dr. Gary Meyers<br>NORPAX A-030<br>Scripps Institution of Oceanography<br>La Jolla, California 92093 | 1 |
| 11. | Prof. Klaus Wyrtki<br>Institute of Geophysics<br>University of Hawaii<br>Honolulu, Hawaii 96822 | 1 |

182800

Thesis
L546 LeRoy
c.1 Tropical disturbances in an oceanic general circulation model with seasonal forcing.

182800

Thesis
L546 LeRoy
c.1 Tropical disturbances in an oceanic general circulation model with seasonal forcing.

Tropical disturbances in an oceanic gene
3 2768 002 11847 3
DUDLEY KNOX LIBRARY